THE LARGE-SCALE DISTRIBUTION OF NEUTRAL HYDROGEN IN THE GALAXY

W. B. Burton
National Radio Astronomy Observatory

THE LARGE-SCALE DISTRIBUTION OF NEUTRAL HYDROGEN IN THE GALAXY

W. B. Burton
National Radio Astronomy Observatory

Lecture notes, summer 1972

Chapter 4, "Galactic and Extragalactic Radio Astronomy"

THE LARGE-SCALE DISTRIBUTION OF NEUTRAL HYDROGEN IN THE GALAXY

I. OBSERVATIONS OF NEUTRAL HYDROGEN

Hydrogen is the main constituent of the interstellar medium, and the physical characteristics of the hydrogen are closely related to the characteristics of other galactic constituents, both stellar and interstellar. The interstellar medium is transparent enough to hydrogen radio emission that, with a few directions excepted, investigation of the entire Galaxy is possible. This transparency allows investigation of regions of the Galaxy which are too distant to be studied optically. Interstellar neutral hydrogen is so abundant and is distributed in such a general fashion throughout the Galaxy that the 21-cm hyperfine transition line has been detected in emission in every direction on the sky at which a suitably equipped radio telescope has been pointed. No time variation of a neutral hydrogen line has been found. What we detect is a line profile giving intensity, usually expressed as a brightness temperature, as a function of frequency. The frequency measures a Doppler shift from the natural frequency of 1420.406 MHz. In practice the measured frequency shifts are converted to radial velocities (1 km s^{-1} = -4.74 kHz), and, in Milky Way studies, corrected to the local standard of rest defined by the standard solar motion.

Table 1 lists the main surveys which have been made for galactic-structure studies and published since 1966. Kerr (1968) gave a similar table for surveys carried out before then. These tables summarize the equipment parameters, the region surveyed, and the form in which the results are published. By way of example, reference will be made in this

chapter to the observations shown in figure 1 as a velocity-longitude contour map of neutral hydrogen brightness temperature isotherms. These observations were made along the galactic equator at half-degree longitude intervals between $\ell = -6°$ and $\ell = 120°$.

Profiles observed near the galactic plane typically extend over about 100 km s^{-1}. Broadening in the profiles occurs through several mechanisms. Consequently, the observing bandwidth is chosen according to the type of investigation, taking into account also that the sensitivity varies as $(\text{bandwidth})^{-1/2}$. The intrinsic atomic half-width of the line is 10^{-16} km s^{-1} and is thus infinitesimally small compared to what can be measured by radioastronomical methods and compared with the other causes of broadening. The broadening corresponding to the thermal velocities of atoms within a single concentration of gas will produce a line with a Gaussian shape characterized by a dispersion $\sigma \approx 0.09 \sqrt{T}$ km s^{-1}. For a kinetic temperature of 100 K, $\sigma = 0.9$ km s^{-1} which corresponds to a full width between half-intensity points of 2.1 km s^{-1}. Turbulent motions within a concentration of neutral hydrogen will also produce profile broadening of this order of magnitude. Large-scale streaming motions with amplitudes of the order of 10 km s^{-1} have been observed in a number of regions of the Galaxy, and these motions produce corresponding broadening. But none of these broadening mechanisms is sufficient to account for the observed characteristic widths of 100 km s^{-1}, although these mechanisms will account for much of the structure within a profile. Most of the total broadening comes from differential galactic rotation. This is of particular importance because it means that 21-cm profiles can be interpreted to give information about differential galactic rotation.

II. KINEMATICS OF GALACTIC NEUTRAL HYDROGEN

A. Velocities Due to Differential Galactic Rotation

If the motions of the concentrations of hydrogen gas were governed only by gravitational forces and if the total galactic mass distribution were axially symmetric about the center of the Galaxy, then the gas would be moving in circular orbits. Although it is clear that reality is more complicated, in order to interpret the observations in terms of large-scale structure it has been common to assume that the motions are everywhere circular and that the angular velocity about the center of the Galaxy, $\omega(R)$, is a decreasing function only of distance, R, from the center of the system. We write ℓ for galactic longitude and θ for galactocentric azimuth, both angles being measured as in figure 2. The distance from the observer to the emitting concentration of hydrogen is r. The observer is of course located in the system, at a distance R_o from its center, and is rotating about this center with angular velocity ω_o. The velocity which is measured, V, (by convention positive in sign if the emitting gas is moving away from the observer) is the Doppler shift velocity of the gas along the line of sight:

$$\begin{aligned} V &= \text{component of } \omega R \text{ along line of sight - component of } \omega_o R_o \text{ along line of sight.} \\ &= \omega R \cos (90° - \ell - \theta) - \omega_o R_o \cos (90 - \ell) \qquad (1) \\ &= \omega R (\sin\theta \cos\ell - \cos\theta \sin\ell) - \omega_o R_o \sin\ell. \end{aligned}$$

Which, since $r \sin\ell = R \sin\theta$ and $R \cos\theta = R_o - r \cos\ell$, becomes

$$V = R_o [\omega(R) - \omega_o] \sin\ell. \qquad (2)$$

This is the fundamental equation of 21-cm galactic structure analysis. If the function $R_o\,[\omega(R) - \omega_o]$ is known, then in principle distances along the line of sight can be attributed to each measured V. It is worth emphasizing that distances are not determined directly, but require accurate knowledge of the velocity-field throughout the Galaxy.

Practical application of equation (2) raises a number of problems. The first of these involves the accuracy with which the angular-velocity rotation curve $\omega(R)$ can be determined. Within the framework of the assumptions of the preceding paragraph this can be determined from 21-cm measurements for regions along the line of sight where $R < R_o$, as follows. For any reasonable rotation law V will vary as shown schematically in figure 3. Consider a particular line of sight with ℓ in the range $0° < |\ell| < 90°$. As the distance from the Sun, r, increases along this line of sight, the distance to the galactic center at first decreases. This corresponds to increasing $\omega(R)$ and thus to increasing $|V|$. However, as r increases further a point on the line of sight is reached which is closest to the galactic center. At this "subcentral point", $R = R_{min} = R_o \sin |\ell|$, and $\omega(R)$ and thus $|V|$ reach maximum values. For still larger r, R increases so that $|V|$ decreases from the value it reached at the subcentral point. By measuring the cut-off value of $|V|$ on a profile observed at each longitude and attributing this "terminal velocity" to the distance from the center, $R_o \sin |\ell|$, corresponding to that longitude's subcentral point, one obtains $\omega(R)$ provided R_o and ω_o are known from other methods. The terminal velocity, which is thus $V_T = R_o\,[\omega(R_o \sin |\ell|) - \omega_o] \sin \ell$, is in practice taken as a suitably defined point on the high velocity edge of each profile. The linear-velocity rotation curve, giving the circular velocity $\Theta(R) = \omega R$ as a function of T, is then obtained using

$$\Theta\,(R_o \sin|\ell|) = V_T + \omega_o R_o \sin|\ell|. \qquad (3)$$

Note that this terminal velocity method can not be used for $R > R_o$. As we penetrate along any line of sight in the longitude range $90° < |\ell| < 180°$, R (which in these directions will always be greater than R_o) gets larger and larger so that $\omega(R) - \omega_o$ gets more and more negative and V increases or decreases smoothly, depending on the sign of sin ℓ. There is no unique velocity corresponding to a known unique distance, as there is for the directions $0° < |\ell| < 90°$. Because of this the rotation curve for $R > R_o$ is not derived directly from the 21-cm observations. From the 21-cm rotation curve at $R < R_o$, which is assumed to represent only gravitational forces, a model of the mass distribution of the Galaxy is constructed (see Schmidt 1965), and the rotation at $R > R_o$ is in turn derived from this dynamical model.

In practice the method fails at directions closer to that of the galactic center than $|\ell| \approx 20°$, where the assumption of circular rotation is clearly violated. The method is also weak at longitudes $75° < |\ell| < 90°$: because of the geometry in these directions R, and thus V, change very slowly with increasing distance along the line of sight. Consequently the rotation curve of our Galaxy is best determined from 21-cm observations over the range $4 < R < 9$ kpc. Optical observations, especially of OB stars, provide additional kinematic information for the region where $R \approx R_o$. The comparison of spectroscopically determined optical distances with kinematically determined radio distances is difficult because optical distances are most accurate close to the Sun, where the accuracy of the kinematic distances is poor.

The rotation curve derived by Shane and Bieger-Smith (1966) from observations in the first quadrant of galactic longitude is shown in figure 4. We will see in the following section that the irregularities in this rotation curve can be attributed to large-scale streaming motions. Over much of the Galaxy the deviations from circular velocity are of the order of 5% of the rotation velocities. In the central region where $R < 4$ kpc the non-circular motions are on the same order as the rotation velocities.

It is also clear from figure 4 that over much of the Galaxy Θ changes much more slowly with respect to R than would be the case for solid body rotation. This strong differential rotation indicates a strong increase in total mass towards the center of the galactic system.

It is sometimes useful to have available a simple analytic expression for the rotation curve freed of the perturbations of streaming motions. The expression

$$\Theta\ (R) = R\ \omega(R) = 250.0 + 4.05\ (10-R) - 1.62\ (10-R)^2 \qquad (4a)$$

is a satisfactory fit to the apparent curve in figure 4. It is valid for the region $4 < R < 10$ kpc in the first quadrant of galactic longitude. For the extrapolated region $10 < R < 14$ kpc, a fit to the rotation required by the Schmidt (1965) mass model is given by

$$\Theta\ (R) = R\ \omega(R) = 885.44\ R^{-1/2} - 30000\ R^{-3}. \qquad (4b)$$

Velocities with respect to the local standard of rest, calculated from equation (2) using the velocity-field described by equation (4), are plotted as a function of distance from the Sun in figure 5. This figure illustrates in more detail the points illustrated schematically

by figure 3. Thus it shows the "distance ambiquity" at positive velocities, the unique distance corresponding to the maximum velocity at each longitude in the first quadrant, and the particularly slow variation of velocity with increasing distance at longitudes $75° < \ell < 90°$. If one trusts the rotation curve given by equation (4) and if the radial velocity of a feature is known, then this figure can be used to estimate its distance. For example, at $\ell = 30°$ a radial velocity of $V = +75$ km s^{-1} places the feature at a distance of either 5.3 or 12.0 kpc from the Sun.

Since the observer is located inside the Galaxy and is rotating with it, we must have information on his position in the Galaxy, R_o, and on his rotational velocity, $\Theta_o = \omega_o R_o$, in order to fix the scale and zero-point of the rotation curve. The determination of these basic quantities has been discussed by Schmidt (1965). The distance to the center of the Galaxy can be measured directly by finding the distance to the density maximum of some type of object, such as RR Lyrae variable stars, observed in directions near that of the galactic center. A distance $R_o = 10$ kpc has been adopted as standard, although the determination is sensitive to the correction for interstellar absorption and to the adopted absolute magnitude of the RR Lyrae stars. The rotation velocity at the Sun, Θ_o, is best determined not directly but rather in terms of the Oort constants of galactic rotation A and B. These constants are defined as

$$A \equiv 1/2 \left[\frac{\Theta_o}{R_o} - \left(\frac{d\Theta}{dR}\right)_{R_o}\right] = -1/2\, R_o \left(\frac{d\omega}{dR}\right)_{R_o} \qquad (5a)$$

and

$$B \equiv -1/2 \left[\frac{\Theta_o}{R_o} + \left(\frac{d\Theta}{dR}\right)_{R_o}\right], \tag{5b}$$

so that $\Theta_o = (A-B)\, R_o$. The values of these constants which have been adopted as standard by the I.A.U. (1966) are

$$A = 15 \text{ km s}^{-1} \text{ kpc}^{-1} \tag{6a}$$

and

$$B = -10 \text{ km s}^{-1} \text{ kpc}^{-1}, \tag{6b}$$

so that $\Theta_o = 250$ km s^{-1}, with the uncertainty in the value of Θ_o coming in the first place from the uncertainty in the value of B. It is not easy to measure the error in the quantities Θ_o and R_o; a 20% error can not be ruled out. A subsequent revision of these two quantities will change the scale of the rotation curve, but the shape of it and general kinematic conclusions drawn from it will not be effected.

The 21-cm observations can provide a determination of the <u>product</u> AR_o. Measurement of this product gives a valuable independent check of the values of A and R_o determined separately by other methods. The 21-cm observations provide AR_o as follows. The angular velocity $\omega(R)$ is expanded in a Taylor approximation:

$$\omega(R) = \omega_o + (R-R_o) \left(\frac{d\omega}{dR}\right)_{R_o}. \tag{7}$$

This first-order approximation is good where $R-R_o$ is small. The correction for the second-order term is on the order of 5%. Using the definition of the Oort constant A,

$$\omega(R) = \omega_o - (R-R_o) \frac{2A}{R_o}, \tag{8}$$

so that substitution in equation (2) gives

$$V = -2A\ (R-R_o)\ \sin \ell. \qquad (9)$$

Still assuming circular rotation, there is no distance ambiguity for the terminal velocity, V_T, since this velocity corresponds to $R = R_{min} = R_o \sin |\ell|$. Consequently measurements of the terminal velocities give

$$AR_o = V_T\ [2 \sin \ell\ (1 - \sin |\ell|)]^{-1}. \qquad (10)$$

The product should be determined from observations at longitudes not too much less than 90° in order for the assumption $R \simeq R_o$ to remain valid. The variations observed in V_T, which are of the order of 5 km s^{-1} and attributed to systematic streaming motions, will introduce large errors in AR_o since the denominator in equation (10) is less than 1. Nevertheless, 21-cm determinations of AR_o lie in the range 135 to 150 km s^{-1}, consistent with the adopted values of A and R_o.

Using these values of R_o and Θ_o, the period of revolution of the local standard of rest around the galactic center is $2\pi\ R_o/\Theta_o = 2.5 \times 10^8$ years. This is only 1 or 2 per cent of the age of the galactic disk. How structure in the disk is maintained against the shearing forces of the strong differential rotation for times longer than one galactic revolution has remained a puzzle.

B. Deviations from Circular Symmetry and Circular Motions

One assumption which is important in the rotation curve derivation is the assumption that there is enough hydrogen present near the subcentral point to actually determine the cut-off of the profile. Suppose there is

not enough hydrogen there; then the measured terminal velocities would be contributed by gas in a region with $R > R_o \sin|\ell|$ and thus $\omega < \omega$ $(R_o \sin|\ell|)$ so that the derived $\Theta(R)$ would be less than the true velocity. In fact, the observed rotation curve plotted in figure 4 shows irregularities in the velocities plotted against distance from the center. In the original determination of the rotation curve by Kwee, Muller and Westerhout (1954), this sort of irregularity was attributed to extended regions that did not contain enough gas near the subcentral point to determine the profile cut-off. The idea was that if there was not much gas at the subcentral point, the observed cut-off velocity would be due to lower velocity gas at $R > R_o \sin|\ell|$. If this is the case, then the rotation curve should be drawn using the upper envelope of the observed terminal velocities. Circular motion could in this way be retained. However, Shane and Bieger-Smith (1966) showed that the irregularities could better be attributed to large-scale streaming motions, that is, to systematic deviations from circular rotation. They rejected the possibility of large empty regions because low-intensity extensions on the ends of profiles are not observed at longitudes corresponding to the dips in the run of observed terminal velocities. A model based on <u>circular</u> rotation and reproducing most characteristics of the terminal velocities could only be constructed by using an unacceptably artificial density distribution. In order for the whole maximum velocity part of the profile to shift to lower velocities there would have to be essentially no hydrogen (about a factor 100 less than the average hydrogen density) along the whole region of the line of sight within approximately 10 km s^{-1} of the velocity corresponding to the

subcentral point. This means (as is clear from inspecting figure 5), that regions of 4 or 5 kpc extent would have to be essentially empty of gas, and that these regions would have to have a preferential orientation with respect to the observer. This is implausible. The conclusion that the observed irregularities in the run of the terminal velocities reflect corresponding irregularities in the galactic velocity-field is an important one.

There are other indications that the assumption of circular rotation is less than satisfactory. Unambiguous proof of noncircular motions in the Galaxy is given by profiles observed in the galactic plane in the cardinal directions $\ell = 0°$, 90° and 180°. The velocities expected in terms of circular rotation at these longitudes are illustrated in figure 5, while figure 6 shows the profiles observed. At longitudes 0° and 180°, all circular motions would be perpendicular to the line of sight, and in the presence of only such motions the profiles would have one peak symmetric with respect to zero velocity. Actually, strong radial motions are observed. For $\ell = 90°$, circular motion would imply no positive velocity peak in the profile. Actually, there is a peak at $V \simeq +6$ km s^{-1}.

Since there is no reason to expect these irregularities to be axially symmetric, or even to have characteristic length scales of more than a few kiloparsecs, the rotation curve illustrated by the wavy line in figure 4 is an <u>apparent</u> one only, since it describes motions along one particular locus, and not over the entire galactic plane. This locus is not necessarily the locus of subcentral points since in the presence of deviations from circular motion the terminal velocity does not necessarily originate at the subcentral point. Thus it is not surprising that the

apparent rotation curve derived from observations of the terminal velocities in the longitude quadrant $-90° < \ell < 0°$ has irregularities somewhat differently placed, although of about the same amplitude. What is more disturbing is that the unperturbed or basic rotation curve, obtained by drawing a smooth curve through the irregular apparent one, is different when determined for the fourth quandrant than when determined for the first quandrant. A pair of apparent rotation curves obtained on the two sides of the galactic center is shown in figure 7. The systematic difference of about 10 km s^{-1} between the two curves over the regions $30° \lesssim |\ell| \lesssim 53°$ is further evidence requiring us to accept kinematic asymmetries on a very large scale.

Deviations from circular symmetry in our Galaxy can be demonstrated in more detail by comparing the cut-offs on both the positive- and negative-velocity wings of profiles observed at the corresponding longitudes ℓ and $-\ell$. Such a comparison is shown in figure 8. The differences in the cut-offs at corresponding longitudes are large and systematic. The cut-offs plotted in figure 8 provide information from different parts of the Galaxy. Although different explanations may have to be found for each region, explanations in terms of kinematics seem more plausible than explanations in terms of the density distribution.

These deviations from circular symmetry have important consequences for the derivation of the galactic distribution of the neutral hydrogen. These consequences are the subject of section III B.

C. Non-Circular Motions Predicted by the Linear Density-Wave Theory

The density-wave theory of galactic rotation has had some success in explaining the observed velocity characteristics of the Galaxy. It

also provides a plausible mechanism for maintaining spiral structure against the strong shearing forces of differential rotation. The theory is discussed in detail in a monograph by Lin and Shu (1973), but it is useful to briefly describe here the observable consequences of the theory.

Spiral arms are considered as waves in the theory. Stars and gas move through the spiral arms, but since they stay longer in the arms, the arms are density maxima. The theory provides for the maintenance of such density waves, although it does not provide for the origin of them. There is still little agreement on the origin of the spiral perturbation in the first place. A density wave of spiral form is assumed to be superimposed as a perturbation on an axisymmetric background mass distribution. The superimposed wave pattern moves relative to the material, with a constant angular velocity Ω_p, and thus does not follow differential rotation. The resultant spiral gravitational field produces streaming motions and a subsequent redistribution of densities which can maintain the imposed perturbation. Although the imposed perturbation is only a few per cent of the total mass density, the interstellar gas responds quite strongly to it. In the linear theory, the effect of the wave on the gas and on the stars is in phase; the effect differs only in the amplitude of the perturbation. According to the theory the response of a particular population of the galactic mass is determined by the population's velocity dispersion. The interstellar hydrogen is characterized by velocity dispersions of about 5 km s^{-1} whereas most of the mass is contributed by older stars with dispersions characteristically almost an order of magnitude larger. Thus for the gas component the theory predicts both large peculiar velocities, typically 7 km s^{-1}, and a large ratio between the density

in the arm and interarm regions of about 3:1. Such streaming motions or such density variations would, by themselves, have easily observable consequences in the profiles. Since in fact such effects are superimposed on top of each other, separating the kinematic from the density characteristics represented in the profiles is a challenging problem.

The density-wave theory relates the streaming motions and the densities as follows. The deviations from circular motion are expressed in terms of the peculiar motions, V_R and V_θ, taken, respectively, to be positive in the directions of increasing radius and azimuth. These peculiar motions are assumed to vary periodically:

$$V_R = -a_R \cos\,(\chi(R, \theta)),$$
$$V_\theta = a_\theta \sin\,(\chi(R, \theta)), \tag{11}$$

where $\chi(R, \theta) = 2\theta - \phi(R)$ is the phase of the superimposed spiral gravitational potential, and $\phi(R)$ is the radial phase function. The amplitude functions of the peculiar motions are given by Lin et al. (1969) in terms of the density contrast between the gas surface density in a unit column perpendicular to the galactic plane through the center of a spiral arm, σ_{max}, and the gas surface density between arms, σ_{min}:

$$a_R = \frac{\sigma_{max} - \sigma_{min}}{\sigma_{max} + \sigma_{min}} \left(\omega(R) - \omega_p\right) \frac{2}{-k(R)},$$
$$a_\theta = \frac{\kappa^2}{4} \frac{1}{(\omega(R))^2 - \omega(R)\omega_p} a_R. \tag{12}$$

Here $\omega(R)$ is the basic unperturbed rotation of the background mass, such as given by equation (4). The superimposed pattern has the form of a two-arm trailing logarithmic spiral rotating with constant angular velocity, ω_p, with respect to an inertial system. The epicyclic frequency, κ, is defined by

$$\kappa^2 = (2\,\omega(R))^2\,(1 + \frac{R}{2\omega(R)}\,\frac{d\omega}{dR}). \tag{13}$$

The radial wavenumber of the spiral pattern is $|k(R)|$, where $k(R) = \frac{d\phi}{dR}$. The spacing between adjacent arms is $\lambda = 2\pi/|k(R)|$.

The geometry of the spiral pattern, $R(\theta) = R_o \exp(-t(\theta-\theta_o))$, is characterized by a tilt angle, t, defined as the acute angle between the spiral and a galactocentric circle (positive in sign for trailing arms). The tilt angle is related to the wave number by

$$k(R) = \frac{\partial\chi}{\partial R}\Big|_\theta = \frac{d\phi}{dR} = 2\,\frac{\partial\theta}{\partial R}\Big|_\chi = -\frac{2}{R\tan t}\,. \tag{14}$$

These equations determine the streaming motions predicted by the first-order density-wave theory for certain assumed parameters, which with certain restraints may be adjusted in accordance with the observations. The sense of the streaming is apparent from (12), since both a_R and a_θ are always positive for $k(R)<0$ (trailing arms) and for $\omega_p < \omega(R)$. For our own Galaxy, the predicted radial velocity with respect to the local standard of rest becomes, in the presence of the density-wave peculiar motions,

$$V(R,\ell,\theta) = V(R,\ell) - V_R\cos(\ell+\theta) + V_\theta\cos(90°-\ell-\theta). \tag{15}$$

Here $V(r, \ell)$ is the unperturbed basic rotation described by equation (2). The density-wave streaming motions relative to the local standard of rest, given by the two righthandmost terms in equation (15), are plotted in figure 9. Indeed it is qualitatively understandable that a stretched-out structural feature will, by its own gravitational forces, induce streaming motions in the sense indicated. Material on the outer side of the feature will be pulled towards it, increasing the material's angular momentum and thus increasing its velocity in the direction of rotation. The situation will be the other way around for material on the inner side of such a feature.

The density-wave theory is valid over the range of the galactic disk for which the conditions

$$\omega(R) - \frac{\kappa}{2} < \omega_p < \omega(R) + \frac{\kappa}{2} \qquad (16)$$

are satisfied. The pattern speed ω_p has been chosen by Lin et al. so that this range is as large as possible. At the borders of this range are the locations of the so-called Lindblad resonances. According to the theory the pattern ends here as a ring. Outside this range the theory is no longer applicable, and so far it is not completely clear what the observational consequences of these resonances would be. For our own Galaxy and a pattern speed of 13 km s^{-1} kpc^{-1}, the inner Lindblad resonance occurs at $R \simeq 3$ kpc. It has been suggested that resonance phenomena might be able to account for the large radial motions observed in the 21-cm line near the "3-kpc arm" (Shane 1972, Simonson and Mader 1972).

The density-wave theory has been applied in some detail to the interpretation of the velocity and density patterns observed in the Milky Way. Streaming motions of the sort predicted by the theory and illustrated by figure 6 have been observed in the gas (Burton 1966, 1971, 1972; Burton and Shane 1970; Shane 1972; Tuve and Lundsager 1972) and in the youngest stars (Humphreys 1970, 1971, 1972). Deriving an apparent rotation curve, using equation (15) and best-fit density-wave parameters, results in the dashed curve labelled "model" in figure 4. This calculated rotation curve is certainly a better fit to the one derived from the first-quadrant observations than the one derived using the circular rotation equation (2). The theory has also been used to interprete observations of a few external galaxies (M101, Rogstad 1971; M51, Mathewson et al. 1972).

III. DETERMINATION OF GALACTIC STRUCTURE

The standard overall picture of the neutral hydrogen distribution in the Galaxy is still the one based early Dutch and Australian observations (Schmidt 1957, Westerhout 1957, Kerr 1962). This map, shown in figure 10, was derived using the basic equation (2). We have seen that the assumptions of axial symmetry and circular rotation inherent in this equation are not generally valid. It now remains to be seen how this should influence the interpretation of the standard map in figure 10, and to discuss some of the problems involved in the derivation of such a map.

A. Line Profile Characteristics Caused by Geometrical Effects

It is instructive to look in more detail at the change of V with distance along the line of sight calculated for the simple circular rotation described by equation (4). This velocity with respect to the local standard of rest is plotted (using a full-drawn curve) against distance from the Sun for two typical longitudes, $\ell=50°$ and $\ell=75°$, in figure 11a.

Two things are immediately evident from this figure. In the first place, there are two regions on the line of sight which contribute to each positive velocity, whereas only one region contributes to each negative velocity. This distance ambiguity is expected in all directions where $|\ell| < 90°$. If the hydrogen gas is optically thin and generally distributed throughout the Galaxy, the effect of this double-valuedness at positive velocities (for $0° < \ell < 90°$) should show up in the observations since the intensities at positive velocities should then typically be about twice what they are at negative velocities. The actual existence of the intensity cut-off near zero velocity in the range $20° < \ell < 70°$, evident in the reference map in figure 1, indicates that on the largest scale the hydrogen gas at these longitudes is indeed optically thin. In the second place, figure 11a shows that the velocity observed from regions near the subcentral point changes relatively slowly along the line of sight. Consequently the profiles contain, near the terminal velocity, a contribution from an especially long path-length. This crowding in velocity results in the high-velocity ridge pattern, which is a striking characteristic of the observations in the reference map.

The number of hydrogen atoms in a column of 1 cm^2 cross-section per unit interval of velocity is $n_H \left(\left|\frac{dV}{dr}\right|\right)^{-1}$, where n_H is the density

of hydrogen atoms per cubic centimeter. Assuming that the hydrogen is more or less evenly distributed, the relative contribution to the profiles at each velocity is determined by the rate of change of the velocity with distance. This is illustrated by figure 11b. Here the change of velocity with distance from the Sun, $|\frac{dV}{dr}|$, summed at positive velocities where there is the distance ambiquity between the near and the far side of the subcentral point, is plotted against velocity. The vertical scale is $|\frac{dV}{dr}|$, but, since intensities at velocities at which $|\frac{dV}{dr}|$ is small will be proportionately enhanced on the profiles, the vertical scale can be interpreted as an intensity scale. Thus the plots in figure 11b can be considered schematic line profiles.

The full-drawn curves in figure 11 are calculated for simple circular rotation. The dashed curves in the figure, however, are calculated for a rotation law in which large-scale streaming motions are present. At this stage it is not important that the rotation law used is one derived using density-wave theory kinematics and illustrated in figure 4. What is important is that in the presence of deviations from circular motion, the variation of V along the line of sight will not be as regular as in the circular rotation case but will show the sort of structure illustrated in figure 11a. Irregularities in the plot of V against r will show up as structure in the schematic profile constructed from the $|\frac{dV}{dr}|$ against r relation.

Theoretical line profiles which represent the geometrical effects in a more realistic way can be calculated assuming a rotation law and a completely uniform hydrogen distribution. Such profiles are shown in figure 11c. The full-drawn profiles are calculated for the circular rotation described by equation (4), for $\ell = 50°$ and $\ell = 75°$. These

calculated profiles illustrate that structure in the observed profiles is to be expected even for a structureless distribution of hydrogen throughout the Galaxy. The cut-off near zero velocity, due to the fact that two regions contribute to positive velocities, and the enhanced intensities near the maximum velocity, due to the crowding in velocity near the subcentral point, are geometrical effects which are model independent in the sense that structure of this sort would be present in the profiles for any reasonable rotation law and density distribution. Obviously, this sort of profile structure must be satisfactorily accounted for in the subsequent analysis of profiles and not attributed to spurious characteristics of the hydrogen distribution. Although there are numerous cases in the literature where this has not been done, it should not be too difficult to account for the model-independent effects.

Accounting for the effects of systematic streaming motions is a different matter, however. The dashed-line profiles in figure 11c were calculated using the density-wave theory velocity-field illustrated by figure 11a and, again, a completely uniform hydrogen distribution. The profiles show the model-independent effects, but these effects are now superimposed on the geometrical effects attributable to deviations from circular rotation. The dashed-line profiles illustrate the efficiency with which systematic streaming motions of about 5 km s^{-1} amplitude will distort the observations; it would require large density differences to achieve intensity differences equivalent to those obtained by systematic streaming motions of only a few km s^{-1}. The observed profiles are included in figure 11c, as dots, in order to show that the structure in the observed profiles is of the same magnitude as the structure in the calculated profiles.

B. The Kinematic Distribution of the Neutral Hydrogen

It is important to emphasize that profiles are more sensitive to small variations in the streaming motions than to even substantial variations in the hydrogen density (Burton 1971, 1972; Tuve and Lundsager 1972). Line profiles are sensitive to the velocity-field because what is observed is the amount of hydrogen per unit velocity. In the presence of streaming motions, there will be regions on the line of sight where the radial velocity changes relatively slowly with increasing distance from the Sun. The relative contribution to the observed profiles from these regions where $\left|{}^{dV}/_{dr}\right|$ is small will be enhanced. Irregularities in the velocities are themselves sufficient to cause the appearance in the profiles of structure which has generally been interpreted in terms of density concentrations on galactic structure maps derived assuming purely circular rotation.

In order to exploit the fact that line profiles are very sensitive to velocity variations, we can assume for the sake of the argument that all structure in the profiles has a kinematic origin. By adjusting the line-of-sight streaming motions in a model, but maintaining a uniform density and temperature distribution, any profile can be reproduced to within a scale factor. This method of perturbing the line-of-sight velocity field, illustrated in figure 12, involves fitting model profiles to observed profiles by perturbing the line-of-sight velocity field from the basic circular-rotation velocity field described by equation (4). The difference between the perturbed and the basic line-of-sight velocity fields, $V_p - V_o$, gives information on the spatial distribution of the

streaming motions. Application of the method to profiles observed in the galactic plane results in the distribution of the streaming parameter $V_p - V_o$ shown in figure 13. It is clear from this figure that the observations are satisfactorily reproduced with line-of-sight streaming amplitudes of the order of 7 km s^{-1}. This amplitude is about 3% of the velocity of rotation about the galactic center. The sense and magnitude of the kinematic variations are consistent with gas motions observed in a number of regions and with motions predicted by the density-wave theory. The spatial distribution of $V_p - V_o$, provided by the procedure, is a measure which can be compared with optically derived velocity residuals, using optical distances. Optical observations of HII regions, supergiants and Cepheids show streaming motions similar in amplitude and spatial distribution to those derived from the hydrogen observations.

The kinematic approach outlined here is discussed in more detail by Burton (1972) and by Burton and Bania (1973). The detailed interpretation of a map such as the one in figure 13 requires the adoption of a theory relating the velocity and density fields, since it is clear that in fact fluctuations in velocity and in density will accompany each other. In any case, the approach serves to emphasize the extreme sensitivity of the observations to streaming motions.

C. The Model-Making Appraoch to the Derivation of the Large-Scale Structure

Because streaming motions and density variations will generally be associated, attempts to derive the spatial distribution of the gas should be based on simultaneously derived solutions for the galactic velocity-field. We have seen that even slight variations in local velocity conditions can lead to substantial variations in the observed profiles. It

is necessary to account for the consequences of both the adopted velocity-field and density distribution when deriving the large-scale structure. A good way to do this is to calculate model line profiles whenever one produces a map of the galactic structure*. These line profiles would of course contain the effects discussed in section III A inherent in the overall geometry and in the particular velocity-field adopted. It would be very difficult to account for these effects otherwise. Once it is established that the structure map is reasonable in the sense of the comparison of the model profiles with the observations, the map can further be judged in terms of the reasonableness of the adopted velocity-field and resultant density distribution.

Figures 14 and 15 show velocity-longitude contour maps constructed from model line profiles. These maps can be compared with the observed contour map in figure 1. The model in figure 14 was constructed using a velocity-field of the type predicted by the density-wave theory and described by equation (15). The parameters in the density-wave theory formulation were adjusted so that the model contour map agrees as well as possible with the map in figure 1. The resultant streaming amplitudes in this model vary between 3 and 8 km s^{-1}, the arm-interarm density contrast is typically 3:1 and the tilt of the spiral pattern is about 7°.

The map in figure 15 illustrates some of the failures of kinematic models based on circular rotation. This map was constructed using the same density distribution and the same spiral pattern as in the figure 14 model, but using only the basic rotation of equations (2) and (4), without the density-wave theory perturbation. The different appearance between

---

* A procedure for calculating model line profiles has been outlined by Burton (1971).

the models in figures 14 and 15 is due entirely to the difference in the velocity-fields. It is clear that the second model is a poorer fit to the observations.

Figure 16 illustrates the approach in more detail for the interior portion of the Galaxy between $\ell = 40°$ and $\ell = 90°$. The figure is a composite consisting of the observed velocity-longitude contour map (figure 16a), the model contour map which is a best fit to the observations (figure 16b) and the spatial map (figure 16c) illustrating the density distribution used in deriving the model.

The model in figure 16, which is based on density-wave kinematics, is similar to the one in figure 14 in most respects. The fit of the model to the observations is judged by comparing the maps in figures 16a and 16b. The strong intensities near the terminal velocities, the cut-off in intensities near zero velocity, and the enhanced intensities between $\ell \simeq 65°$ and 85° are interpreted in terms of the model-independent effects discussed in section III A. The density-wave theory has been able to account for the run of terminal velocities with longitude, as well as the general appearance of the observations associated with the Sagittarius spiral arm, which is seen tangentially at $\ell \simeq 50°$.

Figure 16c illustrates the space-density distribution which was used as input in deriving the contour map in figure 16b. The shaded part of figure 16c is the region where the density is above average; as has been stressed, the exact density distribution is only important in the model in that it determines the streaming amplitudes through the equations of section II C. The borders of the shaded regions in figure 16c are the loci of maximum $|V_\theta|$ and the loci of $V_R = 0$. In spite of the very

simple spatial distribution input, the resulting agreement with the observations is rather detailed when viewed in the observed velocity space.

D. Some Remarks on the Spiral Structure of the Galaxy

It is clear from figure 11c that any deviations from the adopted rotation law of only 1 or 2 km s^{-1}, which are systematic over a few degrees on the sky, will probably cause serious errors in the interpretation of the profiles. Since the kinematics dominate the appearance of the profiles, interpretation of the structure observed in the profiles in terms of a map of the density distribution requires very accurate knowledge of the velocity-field throughout the Galaxy. However, the velocity-field is only directly measured along a restricted region near the locus of subcentral points. At the same time it is also obvious that structure in the temperature distribution will also result in structure in the observed profiles. Consequently it is necessary to know the temperature distribution on a large scale. Maps of the hydrogen distribution have generally been based on the further assumptions that the temperature of the gas is constant and that the optical depth is low. Although there is abundant evidence that these assumptions are not generally valid, they have been necessary in order for the analysis to proceed.

We saw in the preceding section that streaming motions of the sort known to exist are themselves capable of producing structure in the profiles of the same sort which is observed. This implies that the interpretation of 21-cm profiles in terms of a map of the density distribution

on a galactic scale is, at best, difficult. Even if the peaks in the profiles are correlated with density concentrations, it will be difficult to account for the profile distortions caused by streaming motions and temperature variations in terms of the hydrogen density distribution. Only in the special case of gas concentrations with no systematic streaming, free from the shearing effects of differential rotation, with constant temperature throughout, and isolated from the model-independent geometrical effects can the relative heights or peaks and valleys in the profiles be interpreted directly in terms of a density contrast between "cloud" and "intercloud" regions. Similarly only in such a situation will the measured dispersion be a direct indication of the random cloud velocities. Although such a situation may pertain locally at large distances from the galactic plane, it certainly does not pertain in the plane itself.

In fact, it is not clear if a particular peak in a line profile owes its characteristics to streaming motions, to a density concentration, or to a variation in temperature. Although it is certain that fluctuations in the velocity, density and temperature will accompany one another, the interstellar hydrogen is embedded in such a complicated environment that it does not seem possible to determine, directly from the observations, the relative importance of the variables for each peak or valley in a profile. Near the galactic plane this very complicated environment includes HII regions, supernovae and their expanding shells, regions of star formation, gravitational effects from mass concentrations, and the largly unknown effects of magnetic fields which are probably coupled to the neutral gas by collisions between

the plasma component and the neutral one. Each of these mechanisms can produce differences in the motions, densities and temperatures on a scale large enough to effect the appearance of the profiles and thus of the subsequent map. This means that hydrogen density variations in the galactic plane cannot be determined with any accuracy directly from observations. Similarly it is not possible to determine the true velocity dispersion from observations in the plane.

Irregularities in the velocities are themselves sufficient to cause the appearance of "spiral arms" on maps derived assuming circular rotation. We saw that irregularities in the velocity-field are observed along the locus of subcentral points. If distances are derived using a mean rotation curve such as the curve described by equation (4), then there will be some intensities observed at velocities higher than the rotation velocities. In preparing the map in figure 10, hydrogen contributing such intensities was distributed uniformly over 2 kpc (2.4 kpc if corrected from the old value R_o = 8.2 kpc to R_o = 10 kpc) of line of sight, situated symmetrically with respect to the subcentral point distance (Schmidt 1957).

The region near the subcentral points in the classic map gets relatively low weight also for the following reason. In preparing the map, the distance ambiquity problem for $R < R_o$ was approached by assuming that the hydrogen layer had a constant thickness. By measuring the distribution in latitude at each velocity an attempt was made to separate the material on the near side of the subcentral point, at a distance r_1 from the Sun, from the material on the far side of the subcentral point, at a distance r_2 where it would substend a smaller angle. For the region $\frac{r_2}{r_1} < 1.8$, which is defined on the map in figure 10 by heavy

lines, the method was not considered accurate enough to allow a separation. For lack of any other information, the contributions at r_1 and r_2 were taken equal. The resulting regularity in the region where $r_1 < 1.8$ is therefore probably fortuitous.

Hydrogen associated with small scale regions with peculiar kinematics, such as expanding associations, could also have influenced the appearance of figure 10. Clube (1967) suggested that the unique kinematics of the local system of luminous B stars within 400 pc of the Sun known as Gould's Belt is sufficient to cause the appearance of a spurious structure on a map of the large-scale structure drawn using a velocity-field described by simple circular rotation.

The map of the large-scale hydrogen distribution in figure 10 has to be considered in these terms. The apparent regularity near the locus of subcentral points has low weight. Some other apparently regular features of the map may be spurious. Most of the assumptions upon which the validity of the fundamental equation depends are not strictly correct; even small deviations from the assumed situation can result in substantial errors in the map. However, it should be added that in many cases, even if a peak in a profile owes its prominence to streaming motions, this streaming motion can be seen as a perturbation on the basic rotation described by equation (4). Consequently the distance assigned to peaks using the basic rotation may be correct to the first order.

Even with these reservations, it seems safe to conclude that 21-cm observations do indicate structure on a large-scale in the galactic plane, although it is not immediately clear whether this structure owes its

prominence to velocity, density or temperature fluctuations. In some cases the structure defines extended regions of some kiloparsecs length. These extended regions are situated, roughly, along galactocentric arcs. But, I wonder if we would call this structure spiral structure if we had no knowledge of other galaxies. This is not to imply that spiral structure does not exist in our Galaxy. After all, we do have knowledge of other galaxies and spiral structure is present to some degree in almost all galaxies with sufficient gas in a disk distribuiton. Although an examination of a number of other galaxies in photographs such as those in the Hubble Atlas of Galaxies shows that the structure is more often than not very irregular, in a number of galaxies a general spiral "grand design" emerges from a more or less tangled background structure. Galaxies with such a grand design can be expected to provide much of the information necessary for a confrontation with theories of spiral structure. But it does not seem to me that the 21-cm observations have demonstrated that our Galaxy does, or does not, belong to the galaxies which display such a grand design.

The problem of the origin and maintenance of spiral structure in galaxies is obviously of fundamental importance. To confront theories of spiral structure, observations are necessary which will provide answers to questions which are so far not satisfactorily answered for our own Galaxy. For our own Galaxy we do not have complete answers to the following questions. Does our Galaxy exhibit a "grand design" of spiral structure? If our Galaxy does have more or less regular arms, are these arms trailing or winding with respect to galactic rotation? What pitch angle

and what spacing between arms characterize the structure? What is the density distribution across an arm? What are the motions of the gas between arms? What are the motions and distribution of the gas relative to the stars? Solutions to these spiral structure problems require that distances be determined with an accuracy substantially better than the characteristic width of a spiral feature. This might be 500 pc.

The weakness of our answers to these questions is due, more than to anything else, to our vantage point within the Galaxy. Our vantage point for observing other galaxies is better. It appears that many of the problems which, according to the plans of a decade ago, were to be solved for the Milky Way system using 21-cm methods, can now better be approached through investigations of other galaxies. This requires line receivers of great sensitivity and telescopes of high resolution.

At the same time the Milky Way problems should be investigated using all the material which can be made available. The picture of the Galaxy which will emerge will be a synthesis of information from a variety of studies, which might inlcude: O- and B-type stars and their associations, M-type supergiants, long-period Cepheid variables, the distribution of optical and radio polarization vectors, the distribution of the continuum background radiation, the integrated properties of 21-cm profiles, the information contained in the latitude variations of 21-cm parameters, optical and radio studies of HII regions, and optical and radio studies of absorption lines.

There is also much which can be, and has been, learned about the neutral hydrogen distribution with less accurate distances. This is discussed in the following sections.

IV. THE NEUTRAL HYDROGEN LAYER

Observations of the hydrogen distribution in the z-direction (perpendicular to the galactic plane) have been a source of information for which accurate distances are not necessary. These observations have shown that the gas is confined to a thin and quite flat layer at distances $R < R_o$. In the outer parts of the Galaxy the layer is thicker than in the inner parts and is systematically distorted from the plane defined by $b = 0°$.

This layer can be studied at distances $R < R_o$ by measuring at each longitude the distribution in latitude of the intensities observed near the terminal velocity. At the terminal velocity there is no distance ambiquity so the linear thickness of the layer can be measured. The deviation of the center of mass from the galactic plane defined by $b = 0°$ can also be measured. Studies of this sort have shown that, although structure is present, this structure is confined to a remarkably thin and flat layer at distances from the center less than $R \simeq R_o$. The average full thickness of the layer to half-density points is about 220 pc. This thickness depends on the subcentral point distances which in turn depend geometrically on the distance scale of the whole Galaxy. In the original thickness determination by Schmidt (1957), $R_o = 8.2$ kpc was used. Although subsequent determinations of the layer thickness using telescopes of higher resolution have shown the angular thickness to be somewhat smaller than in the original determination, the revision of the distance scale to $R_o = 10$ kpc allows the characteristic thickness of about 220 pc to be retained. Within the circle $R = R_o$ the deviation of the center of mass

of this layer from the galactic equator defined by b = 0° is less than 30 pc. These quantities can be compared with the diameter of the layer, which is about 30 kpc.

From the general flatness of the central layer inside the solar distance it is evident that systematic motions in the z-direction must be smaller than a few km s^{-1}. The random gas velocities in the z-direction must increase toward the galactic center in order to dynamically maintain the constant layer thickness against the total mass density, which increases strongly toward the center of the Galaxy. In order to maintain constant thickness the velocity dispersion in the z-direction should increase proportionally to $\frac{\partial K_z}{\partial z}$, the derivative near the galactic plane of the gravitational force in the z-direction. This derivative increases by a factor of about 3 between R = 10 kpc and R = 4 kpc. The average random motion in the z-direction at R = 100 pc might be as high as 50 km s^{-1}. We saw in the preceding sections that the actual random gas velocities are difficult to measure near the galactic plane; however there is some evidence that the dispersion increases with decreasing R. Observations of the dispersion will be easier in other galaxies when adequate equipment is available.

The density of the neutral hydrogen gas remains roughly constant over the entire galactic disk, again in contrast to the density of stars, comprising the bulk of the mass of the Galaxy, which increases strongly toward the center.

Although the average thickness of the layer does not vary much in the part of the Galaxy with $R < R_o$, this is not to imply that the layer

is symmetric with respect to b = 0°, either in temperature or velocity characteristics. In particular, velocity shearing motions are commonly observed, but not completely understood.

The characteristics of the central layer in the transition region near $R = R_o$ are difficult to measure because of the superposition of local gas on the parts of all profiles near zero velocity, and because of very poor distance determinations near $R = R_o$.

At distances $R > R_o$ the central gas layer is not centered at b = 0°. In several cases features extend to a height of several kiloparsecs in the direction perpendicular to the plane. These extensions seem to be associated with the spiral structure in the plane. This association with the structure in the plane is evident in the first place because the extensions occur at the same velocity interval as the structure near b = 0°. There is presumably no ambiquity in this velocity association because of the one-to-one correspondence of velocity to distance in the outer regions. (Primarily because of this one-to-one correspondence the parts of the profiles contributed by the outer regions of the Galaxy are simpler in appearance than the parts contributed by the interior regions, although this of course does not imply that the physical structure is simpler.) The example of a high-z extension in figure 17 is at a height of z = 3.5 kpc at b = 10°. The derivation of this height requires that the distance to the arm in the plane is known. However even an error of 3 kpc in this distance will result in an error of only 0.5 kpc in the z-height.

The high-z extensions remain poorly understood. It is natural to ask how the material reached such large distances into the halo, and

once there how it is maintained in the rather narrow velocity slot corresponding to the spiral feature in the plane. It is also difficult to understand how these extensions have preserved their small internal velocity dispersions and not evaporated into the halo. This is all the more enigmatic since it is conceivable that a violent event or events led to the large z-distances in the first place. Oort (1970) has suggested that if the extensions are expelled from the central layer, explosions such as those observed by Hindman (1967) in the Small Magellanic Cloud could be a possible source of energy. It seems clear that the material would return to the central layer under gravitational attraction on a short time scale of about 10^7 years. The inference is that some replenishment or maintenance mechanism is necessary, since it does not seem reasonable to assume that this rather general phenomenon has come about so recently.

Although the observations of these extensions are still scanty, it is known that the extensions show strong asymmetries with respect to the central layer. In the first quadrant the extensions are primarily to positive latitudes. The example in figure 17 shows no corresponding feature on the negative latitude side of the galactic equator. This extension is consistent with a general warping of the central layer. This warping is such that the centroid of maximum neutral hydrogen density is located at positive latitudes in the first longitude quadrant, while it is found at negative latitudes in the fourth quadrant. Figure 18 is a relief map showing the position of the centroid of the hydrogen distribution with respect to the plane $b = 0°$. It is not known to what extent, if any, the total galactic mass participates in this warping. Figure 18

serves as a reminder that the structural properties derived from observations at one latitude, such as the kinematic properties represented in figure 13, may not be representative of the properties at adjacent latitudes.

There have been several theoretical attempts to explain the curious warping of the hydrogen layer. These attempts are reviewed by Hunter and Toomre (1969). Realizing that the Large Magellanic Cloud is at the galactocentric longitude corresponding to the maximum downward bending. Burke (1957) and Kerr (1957) suggested that the bending might be a tidal distortion by the Magellanic Clouds. Although these authors doubted if the Clouds could be massive enough to account for the distortion, others recently reexamined the suggestion and concluded that resonance could build up adequate effects if (and this is a stringent requirement) the Large Magellanic Cloud has remained in a closed orbit around the Galaxy for about 15 revolutions. Habing and Visser (1967) and Hunter and Toomre (1969) also favor a tidal distortion, but one which arose from a single close transit of the Large Cloud. Hunter and Toomre's model requires a passage of the Large Cloud at a distance of about 20 kpc from the center of the Galaxy. It has also been suggested that close passage of the Cloud might be responsible for some spiral-like structure in the Galaxy. Alternative interpretations of the observed warping have been given by Kahn and Woltjer (1959), who suggested that the distortion might be due to a flow of intergalactic gas past the Galaxy, and by Lynden-Bell (1965), who considered a free oscillation mode of the spinning galactic disk.

Although most of the hydrogen is confined to the central layer, it appears that there is a diffuse and structureless component of hydrogen

extending at least several hundred parsecs beyond the main concentrations. The distribution of densities in the central layer in the direction perpendicular to the galactic plane is approximately Gaussian. However, the distribution does deviate from Gaussian in the form of low-intensity wings extending to higher z-distances. A decomposition of individual line profiles into Gaussian components by Shane (see Oort, 1962) has shown evidence for a background envelope of hydrogen with a larger characteristic velocity dispersion ($\approx$ 11 km s^{-1}) and a larger thickness in latitude to half-density points ($\approx$ 700 pc) than exhibited by the more intense structure in the central layer. Emission from this diffuse background shows a much smoother distribution than that shown by the main concentrations of hydrogen nearer the galactic equator. Shane finds at R = 7 kpc a density of 0.01 atoms cm^{-3} at a height of z = 600 pc. This density is about 4% of the density in the plane.

V. NEUTRAL HYDROGEN IN THE GALACTIC NUCLEUS

The nuclei of large galaxies commonly show signs of eruptive activity. A growing body of evidence suggests that an understanding of the phenomena occurring in galactic nuclei is necessary for an understanding of phenomena observed throughout galaxies. The neutral hydrogen in the central region of our own Galaxy has been studied in detail, and although so far no complete dynamical explanation of the observations has been given, a rather clear picture of the kinematics of the central region has emerged.

The reference map in figure 19 shows 21-cm observations made in the galactic plane in the directions $-6° \leq \ell \leq 16°$. What has been called

the "nuclear disk" appears in this map as the narrow ridge of intensities between $\ell = 0°$ and $\ell = 1.°5$, extending through negative velocities to about -210 km s^{-1}. There is a similar ridge on the other side of the galactic center between $\ell = 0°$ and $\ell = +1.°5$, at positive velocities, which although somewhat confused with other material is clearly symmetric with the ridge at negative velocities. This symmetry both with respect to the direction of the center and with respect to zero velocity strongly suggests that the intensities originate in the central region. The angular extent of the disk implies, adopting R_o = 10 kpc, a radius of about 260 pc.

That the velocities in the disk are rotational velocities seems certain in view of the fact that no sign of non-circular motions attributable to the disk is evident at $\ell = 0°$, either in emission or in absorption. The rotational velocity increases very rapidly going out from the center.

The outer boundary of the disk is quite sharp. The map in figure 19 illustrates the structureless appearance of the nuclear disk, especially for the negative velocities which are uncontaminated by foreground or background emission. This smooth appearance, together with the lack of radial motions, implies that the disk has not been disrupted by violent events in the nucleus.

The nuclear disk extends to $\ell \approx \pm 1.°5$. Between $\ell = -3.°5$ and $-4.°5$, centered at V ≈ -240 km s^{-1}, there is another concentration which also has a symmetric counterpart at positive longitudes and positive velocities. This "nuclear ring" also has very sharp boundaries. In particular, the intensities at the uncontaminated negative velocities show that the region

between the nuclear disk and the ring, at $\ell \simeq -3°$, contains relatively little neutral hydrogen. As is the case with the disk, the asymmetry with respect to both $\ell = 0°$ and $V = 0$ km s^{-1} imply that the ring is concentric with the Galaxy. The radius of the ring is about 750 pc, and there appear to be only rotational motions within it.

Rougoor and Oort (1960, see also Oort 1971) have derived the mass density in the nuclear region of the Galaxy, assuming that the motions in the disk and ring are governed by gravitation only. They showed that the velocities observed are approximately the same as the velocities which one would expect if the mass distribution in the nuclear region of our Galaxy would be similar to that inferred for the Andromeda galaxy from the distribution of light. Thus 21-cm observations have given information on the galactic rotation curve not only for the region $R > 4$ kpc but also for the region $R < 750$ pc.

From the angle it subtends in latitude, the linear thickness of the disk between half-density surfaces is estimated to be less than 100 pc at distances closer to the center than about 300 pc but about 230 pc in the outer parts of the disk. The density of observed neutral hydrogen averages about 0.3 atoms cm^{-3} and is remarkable constant over the entire disk. Although the total amount of neutral hydrogen observed within 750 pc is roughly 4×10^6 $M_\odot$, the total amount of hydrogen must be much larger since much of it must be in the form of unobserved hydrogen molecules. The total mass within 750 pc, presumably due for the most part to old and well mixed population II objects, was estimated by Rougoor and Oort to be 2×10^{10} $M_\odot$. The ratio of neutral hydrogen mass to total mass is thus much less in the nuclear region than elsewhere in the Galaxy.

VI. RADIAL MOTIONS IN THE CENTRAL REGION

So far we have discussed regions where the deviations from circular motion are less than a few per cent of the rotational velocities. The situation is fundamentally different in the region outside the nuclear disk, but inside $R \approx 1/3\ R_o$, where non-circular motions of the same order as the rotational velocities are observed.

One of the most regular 21-cm features observed is the expanding "3-kpc arm" (Rougoor and Oort, 1960; Rougoor, 1964). This feature is evident in the figure 19 reference map as the ridge of intensities extending from $\ell = -6°$ at $V \simeq -80$ km s^{-1}, across the Sun-center line $\ell = 0°$ at $V = -53$ km s^{-1}, and blending into other hydrogen at $\ell \simeq 5°$. There is strong absorption at $\ell = 0°$, $V = -53$ km s^{-1}, indicating that this branch of the arm is located between the Sun and the central continuum source Sagittarius A. The negative radial velocity of the absorption dip indicates that the feature has a net expansion away from the center. Because of this expansion motion, the distance scale of the arm can not be measured by the kinematic procedure of section II A. Instead, the distance scale of the feature has been determined geometrically. The feature can be traced to $\ell \simeq -22°$, where it is seen tangentially. Here $R = R_o \sin 22° = 3.0$ kpc if $R_o = 8.2$ kpc (hence the feature's name) or 3.7 kpc if $R_o = 10$ kpc. Admittedly, the longitude at which the feature becomes tangential to the line-of-sight is not very easy to determine. This is nevertheless the only point on the arm at which a distance can be estimated. Its distance from the center at $\ell = 0°$ is therefore uncertain except that it must pass between the Sun and the center.

Considering now the positive velocities, we see at $\ell = 0°$ intensities at velocities up to about +190 km s^{-1}. There is no appreciable absorption at the high velocities, implying that this gas is located on the far side of the central source and expanding away from it. There are a number of different features evident at positive velocities. The distances to these features, and their interconnections, are highly hypothetical because of the lack of distance criteria.

Besides the gas in the plane, there also appears to be considerable gas both above and below the galactic plane which is also moving in a manner forbidden in terms of circular motion (Shane, see Oort 1966; van der Kruit 1970). Although there is no satisfactory way to measure the distance of this gas, the observations suggest that it is moving away from the galactic center in two roughly opposite directions. The mass of the neutral hydrogen involved in these motions is of the order of 10^6 $M_\odot$. One of the most prominent concentrations has a velocity of -130 km s^{-1} at $\ell = 0°$ and a mean latitude of -2°.5. One plausible interpretation of these observations, suggested by Oort (1966) and worked out by van der Kruit (1971), involves gas ejected from the galactic nucleus with a high velocity and at an angle with respect to the galactic plane. The angle under which the ejection took place, 25° to 30°, would have allowed the nuclear disk to survive. According to this model, the material, which has been ejected with velocities of about 600 km s^{-1}, would return to the galactic plane between 3 and 5 kpc from the center, where the expansion would be braked by the central gas layer. In this way, one could account for the velocity structure of the 3-kpc arm in terms of the low angular momentum of this ejected gas.

Other models for the motions will undoubtedly be considered in the future. In particular, the roles of hydrodynamic and magnetic forces in the nuclear region are unknown. It is also conceivable that gravitational resonance mechanisms, predicted by the density-wave theory, could produce effects similar to those observed (Shane 1972, Simonson and Mader 1972). In addition to the 21-cm data, interpretations of the central region will have to also account for the abundance of molecules, such as OH and H_2CO, which is high relative to other regions of the Galaxy. In particular, it is not clear how molecular formation can take place efficiently in the presence of the observed violent motions.

To summarize, it is not clear what mechanism is responsible for the motions observed in the central regions, nor whether only one type of mechanism is responsible for all these motions. It is also not clear if the motions we observe are transient and perhaps rare pehnomena, or if on the other hand we are observing a permanent flow of gas. The flux involved in the gas flow is of the order of 1 or 2 solar masses per year. If the flow is a steady phenomenon a mechanism for a circulation of gas through the center is necessary. What is clear, in view of rapidly accumulating evidence, is that an understanding of the activity in the nuclei of galaxies is of utmost importance.

Burke, B. F. 1957, Astr. J., 62, 90.

Burton, W. B. 1966, Bull. Astr. Inst. Netherl., 18, 247.

Burton, W. B. 1970a, Astr. Astrophys. Suppl., 2, 261.

Burton, W. B. 1970b, Astr. Astrophys. Suppl., 2, 291.

Burton, W. B. 1971, Astr. Astrophys., 10, 76.

Burton, W. B. 1972, Astr. Astrophys., in press.

Burton, W. B., Bania, T. M. 1973, in preparation.

Burton, W. B., Shane, W. W. 1970, The Spiral Structure of our Galaxy, 397-414, (Becker, W., Contoporulos, G., eds., Dordrecht).

Clube, S. V. M. 1967, The Observatory, 87, 140.

Dieter, N. H. 1972, Astr. Astrophys. Suppl., 5, 21.

Gum, C. S., Kerr, F. J., Westerhout, G. 1960, Monthly Notices Roy. Astr. Soc., 121, 132.

Habing, H. J., Visser, H. C. D. 1967, Radio Astronomy and the Galactic System, 159-160, (van Woerden, H., ed., London).

Henderson, A. P. 1967, Thesis, University of Maryland.

Hindman, J. V. 1967, Aust. J. Phys., 20, 147.

Hindman, J. V., Kerr, F. J. 1970, Aust. J. Phys. Astrophys. Suppl., 18, 43.

Humphreys, R. M. 1970, Astr. J., 75, 602.

Humphreys, R. M. 1971, Astrophys. J., 163, L111.

Humphreys, R. M. 1972,

Hunter, C., Toomre, A. 1969, Astrophys. J., 155, 747.

I.A.U. 1966, Trans. I.A.U., 12B, 314-316.

Kahn, F. D., and Woltjer, L. 1959, Astrophys. J., 130, 705.

Kerr, F. J. 1957, Astr. J., 62, 93.

Kerr, F. J. 1962, Mon. Not. Roy. Astr. Soc., 123, 327.

Kerr, F. J. 1968, Stars and Stellar Systems, 7, 575-622, (Middlehurst, B. M., Aller, L. H., eds., Chicago).

Kerr, F. J. 1969a, Ann. Rev. Astr. Astrophys., 7, 39.

Kerr, F. J. 1969b, Aust. J. Phys. Astrophys. Suppl., 9, 1.

Kerr, F. J., Hindman, J. V. 1970, Aust. J. Phys. Astrophys. Suppl. 18, 1.

Kerr, F. J. and Vallak, R. 1967, Aust. J. Phys. Astrophys. Suppl., 3, 1.

Kruit, P. C. van der 1970, Astr. Astrophys., 4, 462.

Kruit, P. C. van der 1971, Astr. Astrophys., 13, 405.

Kwee, K. K., Muller, C. A., Westerhout, G. 1954, Bull. Astr. Inst. Netherl., 12, 117.

Lin, C. C., Shu, F. H. 1973, Monograph on the Density-Wave Theory, in preparation.

Lin, C. C., Yuan, C., Shu, F. H. 1969, Astrophys. J., 155, 721.

Lindblad, P. O. 1966, Bull. Astr. Inst. Netherl. Suppl., 1, 177.

Lynden-Bell, D. 1965, Monthly Notices Roy. Astr. Soc., 129, 299.

Mathewson, D. S., Kruit, P. C. van der, Brown, W. N. 1972, Astr. Astrophys., 17, 468.

Oort, J. H. 1962, Interstellar Matter in Galaxies, 71-77, (Woltjer, L., ed., New York).

Oort, J. H. 1966, Non-stable Phenomena in Galaxies, 41-45, Arakeljan, M., ed., Yerevan).

Oort, J. H. 1970, Astr. Astrophys. 7, 381.

Oort, J. H. 1971, Nuclei of Galaxies, 321-344, (O'Connell, D. J. K., ed., Amsterdam).

Oort, J. H., Kerr, F. J., Westerhout, G. 1958, Monthly Notices Roy. Astr. Soc., 118, 379.

Rogstad, D. S. 1971, Astr. Astrophys., 13, 108.

Rougoor, G. W. 1964, Bull. Astr. Inst. Netherl., 17, 381.

Rougoor, G. W., Oort, J. H. 1960, Proc. Nat. Acad. Sci., 46, 1.

Schmidt, M. 1957, Bull. Astr. Inst. Netherl., 13, 247.

Schmidt, M. 1965, Stars and Stellar Systems, 5, 513-530 (Blaauw, A., Schmidt, M., eds., Chicago).

Shane, W. W. 1971a, Astr. Astrophys. Suppl., 4, 1.

Shane, W. W. 1971b, Astr. Astrophys. Suppl., 5, 21.

Shane, W. W. 1972, Astr. Astrophys., 16, 118.

Shane, W. W., Bieger-Smith, G. P. 1966, Bull. Astr. Inst. Netherl., 18, 263.

Simonson, S. C., Mader, G. L. 1972, Bull. Am. Astr. Soc., 4, No.2, Part 11, 2bb.

Simonson, S. C. and Sancisi, R. 1972, Astr. Astrophys. Suppl., in press.

Tuve, M. A., Lundsager, S. 1972, monograph, Department of Terrestial Magnetism, Washington, in press.

Velden, L. 1970, Beiträge zur Radioastronomie, Max-Planck Institut für Radioastronomie, Bonn, Bd. I, 7.

Westerhout, G. 1957, Bull. Astr. Inst. Netherl., 13, 201.

Westerhout, G. 1969, Maryland-Green Bank Galactic 21-cm Line Survey, 2nd Ed., University of Maryland.

Table 1. Surveys Of Hydrogen Emission From Near The Galactic Equator

Authors	Publication Date	Beam	Bandwidth $\Delta\nu$ (kHz)	Region	Interval	Form of Publication
P. O. Lindblad	1966	°6	10	ℓ = 173° to 243° b ≈ -15° to 2°	irregular irregular	profiles*
A. P. Henderson	1967	10'	8	ℓ = 16° to 230° b = -10° to 10°	$\Delta\ell$ = 5° scanned	$(b, V)\|_{\ell}$ maps
F. J. Kerr and R. Vallak	1967	14!5	38	ℓ = -1° to 1° b = -1° to 1°	$\Delta\ell$ = °1 Δb = °1	$(b, V)\|_{\ell}$ maps
F. J. Kerr	1969b	14!5	38	ℓ = -64° to 63°5 b = 0° ℓ = -60° to 60° b = -2° to 2°	$\Delta\ell$ = °1 $\Delta\ell$ = 1° or 5° Δb = °1	$(\ell, V)\|_{b}$ maps $(b, V)\|_{\ell}$ maps
G. Westerhout	1969	10'	8	ℓ = 11° to 235° b = -1° to +1°	$\Delta\delta$ = 5'	$(\alpha, V)\|_{\delta}$ maps
W. B. Burton	1970a	°6	8	ℓ = -6° to 120° b = 0°	$\Delta\ell$ = °5	profiles and $(\ell, V)\|_{b}$ maps
W. B. Burton	1970b	°6	10	ℓ = 43° to 56° b = -4°5 to 4°5	$\Delta\ell$ = °5 Δb = °5	profiles*, $(\ell, V)\|_{b}$ and $(b, V)\|_{\ell}$ maps
P. C. van der Kruit	1970	°6	50	ℓ = 8° to 10° b = -5° to 5°	$\Delta\ell$ = 1° Δb - °5	$(b, V)\|_{\ell}$ maps
J. V. Hindman and F. J. Kerr	1970	14!5	38	ℓ = -170° to -61° b ≈ -5° to 5°	$\Delta\ell$ = 5° Δb = °1	$(b, V)\|_{\ell}$ maps
F. J. Kerr and J. V. Hindman	1970	14!5	38	ℓ = -175° to 63° b = 0°	$\Delta\ell$ = 1°	$(\ell, V)\|_{b}$ maps

Table 1. Surveys Of Hydrogen Emission From Near The Galactic Equator

(Continued)

Authors	Publication Date	Beam	Bandwidth $\Delta\nu$ (kHz)	Region	Interval	Form of Publication
L. Velden	1970	°6	12	ℓ = 120° to 240° b = -30° to 30°	$\Delta\ell$ = 10° Δb = °5	profiles*
W. W. Shane	1971a, 1971b	°6	20	ℓ = 22°3 to 42°3 b = -6° to 6°	$\Delta\ell$ = 1° Δb = °5	profiles*, $(b, V)\big\|_{\ell}$ maps
N. H. Dieter	1972	°6	10	ℓ = 10° to 250° b = -15° to 15°	$\Delta\ell$ = 2° Δb = 2°	$(b, V)\big\|_{\ell}$ maps
S. C. Simonson and R. Sancisi	1972	°6	16	ℓ = -6° to 24° b -5° to 5°	$\Delta\ell$ = °5 Δb = °5	profiles, $(\ell, V)\big\|_{b}$ and $(b, V)\big\|_{\ell}$ maps
M. A. Tuve and S. Lundsager	1972	°9	10	ℓ = -24° to 270° b = -16° to 16°	$\Delta\ell$ = 4° Δb = 2°	profiles*

* Gaussian decomposition of line profiles available

FIGURE CAPTIONS

Figure 1 Contours of neutral hydrogen brightness temperatures in the galactic plane (Burton, 1970a). Broken-line contours enclose regions of relatively low brightness temperatures. The velocity is with respect to the local standard of rest. The bandwidth (1.7 km s^{-1}) and the half-power beamwidth (0°.6) of the observations are indicated by a cross in the upper right-hand corner. Temperatures in the ranges 70 K < T_b < 90 K, 90 K < T_b < 110 K, and T_b > 110 K are indicated by successive degrees of shading. The dotted portion of the map near $\ell = 0°$, V = 0 km s^{-1} is a region of absorption where contour lines would be overcrowded due to steep temperature gradients. Observations are spaced at half-degree intervals of longitude.

Figure 2 Diagram illustrating the construction used in the derivation of equation (2).

Figure 3 Schematic run of velocities with respect to the local standard of rest as a function of distance from the Sun. For the longitude range $0° < |\ell| < 90°$, the diagram illustrates the distance ambiguity, the terminal velocity and the subcentral point distance.

Figure 4 Apparent galactic rotation curves. The irregular curve is the one derived by Shane and Bieger-Smith (1966) from observations in the longitude range $22° < \ell < 70°$. The smooth

curve is the basic rotation curve which represents the observed one freed of the perturbations of streaming motions. The dashed curve shows the basic rotation curve perturbed by the density-wave theory streamings discussed in section II C. In the presence of deviations from circular motion the maximum velocity might not come from the subcentral point; nevertheless the figure is drawn assuming that it does.

Figure 5 Contours of velocity with respect to the local standard of rest, expected for the circular rotation described by equation (4), plotted as a function of longitude and distance from the Sun.

Figure 6 Line profiles observed in cardinal directions at $b = 0°$, unambiguously showing systematic deviations from circular motion. Because of very strong absorption at $\ell = 0°$, the profile at $\ell = 1°$ is substituted for it.

Figure 7 Apparent galactic rotation curves derived by Kerr (1969a) from observations in the first longitude quadrant (dots) and from observations in the fourth quadrant (crosses). The differences between the two curves imply large-scale deviations from circular rotation.

Figure 8 Comparison of cut-offs on positive- and negative-velocity wings of profiles observed in the longitude range $0° < \ell < 180°$ (dots, right-hand scale) with those in the

corresponding longitudes in the range $180° < \ell < 360°$ (crosses, left-hand scale). The systematic differences in the cut-off velocities imply large-scale deviations from axial symmetry. The data are taken from the surveys of Westerhout (1969) and Kerr and Hindman (1970), as indicated.

Figure 9 Streaming motions relative to the local standard of rest predicted for the gas by the density-wave theory. The contours represent the two righthandmost terms in equation (15).

Figure 10 Distribution of neutral hydrogen densities in the galactic plane as determined from the Dutch and Australian surveys (Oort et al. 1958). This map was drawn using equation (2) (with R_o = 8.2 kpc) and depends for its validity on the validity of the assumptions inherent in that equation. Because of this, the map is difficult to interprete and may contain serious errors. Nevertheless, it seems that it would be difficult to produce an improved version valid over the whole galactic plane.

Figure 11 Diagram illustrating for two typical longitudes the importance of the geometrical velocity-crowding effects for the case of purely circular rotation (full-drawn lines) and for the density-wave velocity-field (dashed lines) which incorporates non-circular motions of about 5 km s^{-1}. (a) Velocity with respect to the l.s.r. as a function of distance

from the Sun. (b) Schematic line profiles each considered as the sum, for the near and far side of the subcentral point, of the slopes $|\frac{dV}{dr}|$ of the corresponding curve in (a). These profiles show the relative geometrical enhancement at each velocity. (c) Theoretical line profiles calculated with the velocity-fields illustrated in (a) and a completely uniform distribution of hydrogen density, temperature and dispersion. The structure in the profiles is attributed to regions along the line of sight where the velocity changes slowly with distance.

Figure 12 Diagram illustrating the kinematic profile-fitting approach for two typical longitudes. (a) Comparison of the observed profiles (dots) with model profiles. The zero-order profile (full-drawn line) was calculated with the basic circular-rotation velocity field $V_o(R_{sun})$ and a completely uniform hydrogen distribution $n_{H_o} = 0.4\ cm^{-3}$. The heavy dashed-line profile was calculated by perturbing only the velocity field, giving $V_p(R_{sun})$, leaving the density uniform. The profile illustrated by the light dashed line was fit to the observations by varying the density, giving $n_{H_p}(R_{sun})$, while retaining the circular velocity field, $V_o(R_{sun})$. (b) Perturbed line-of-sight velocity-field, $V_p(R_{sun})$, which together with a uniform hydrogen distribution results in the heavy dashed-line profile in (a). Note that the kinematic approach can account for the "forbidden-velocity" peak at $\ell = 90°$ in a natural manner and that the required streaming amplitudes appear reasonable.

(c) Perturbed density distribution, $n_{H_p}(R_{sun})$, which together with the circular-rotation velocity field results in the light dashed-line profile in (a). Note that the density approach fails to account for the "forbidden-velocity" hydrogen and that extended, essentially empty, interarm regions are necessary.

Figure 13 Line-of-sight streaming motions derived from observations in the galactic plane using the kinematic procedure illustrated in figure 12. The contour values express in km s^{-1} the difference between the perturbed velocity field and the circular rotation velocity field. These streaming motions alone (thus retaining constant gas density) are sufficient to account for the structure in the observed profiles. This figure was derived from observations kindly provided by Prof. Westerhout.

Figure 14 Model velocity-longitude contour map for the galactic plane based on the density-wave theory.

Figure 15 Model velocity-longitude contour map based on circular galactic rotation and the same hydrogen distribution as derived for the model in figure 14.

Figure 16 Composite diagram illustrating the model line-profile approach for the hydrogen distribution near the galactic plane in the region $40° \leq \ell \leq 90°$. (a) Observed V, ℓ contour map. (b) Model contour map based on self-consistent density-wave streaming and hydrogen distribution, derived as a best-fit to the

observations. Although there is no detailed structure in the input, a certain amount of detailed agreement with the observations is evident after transformation to the observed V, ℓ space. (c) Map of the hydrogen distribution corresponding to the density distribution inherent in part (b) of the figure. The shaded regions are regions of above-average hydrogen density. The emphasis in deriving the distribution is on the agreement of figure 16b with figure 16a, since both of these figures represent the same velocity space.

Figure 17 Contours of antenna temperature in the velocity-latitude plane illustrating for $\ell = 35°$ the deviation of the outer part (at this longitude: negative velocities) of the hydrogen layer from the galactic equator $b = 0°$.

Figure 18 Relief map showing the deviation in parsecs of the position of maximum hydrogen density from the galactic plane (Gum et al. 1960). The indicated longitude is in the old ℓ^{I} system and the distance scale is determined by $R_o = 8.2$ kpc.

Figure 19 Contours of neutral hydrogen brightness temperatures in the plane in directions near that of the galactic center (Burton, 1970a). Broken-line contours enclose regions of relatively low brightness temperatures. The bandwidth (1.7 km s^{-1}(and the half-power beamwidth (0°.6) are indicated by a cross in the upper left-hand corner. The shaded portions of the map are reigons of absorption where contour lines would be overcrowded due to steep temperature gradients. Observations are spaced at half-degree intervals of longitude.

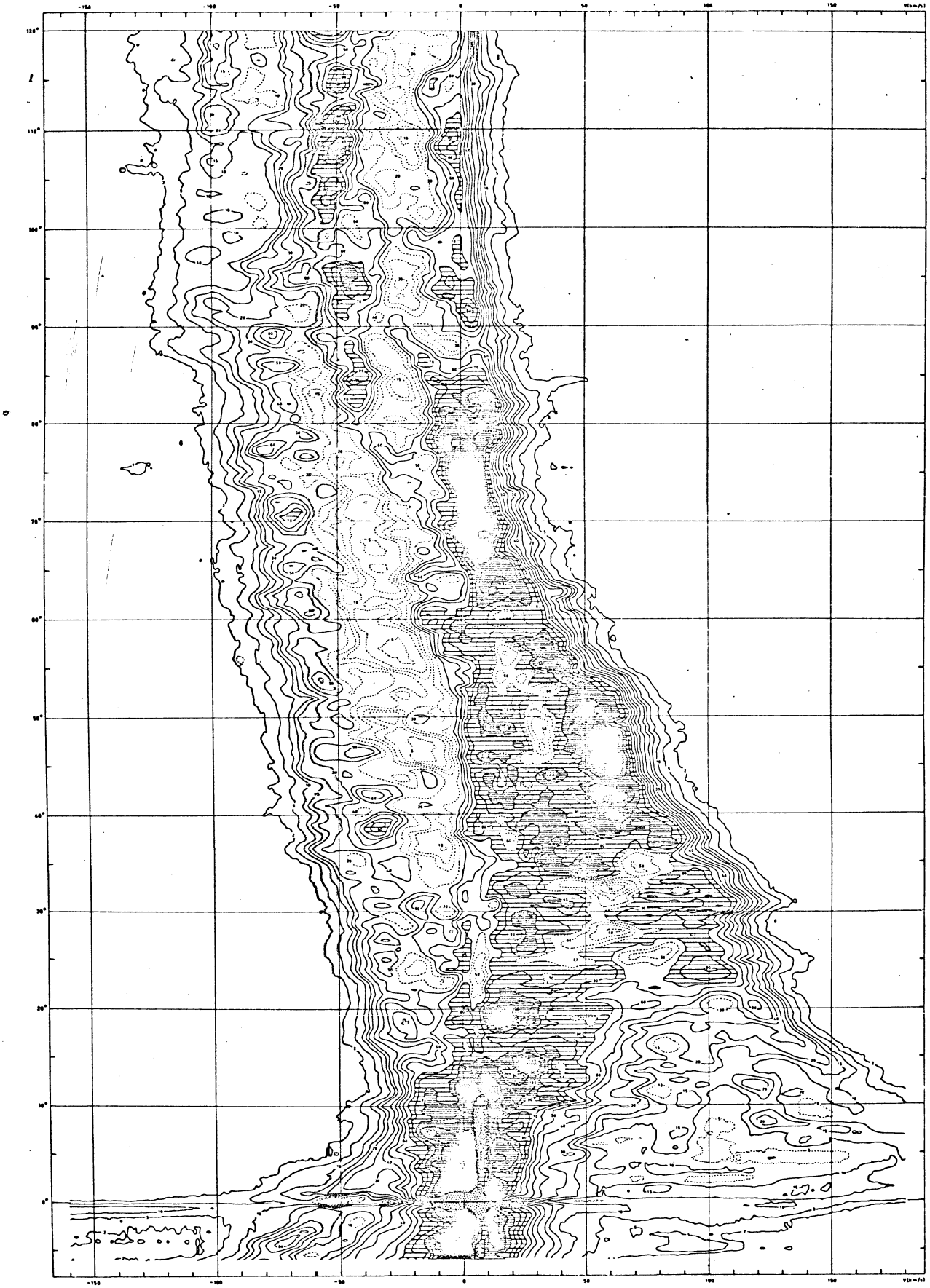

Figure 1.

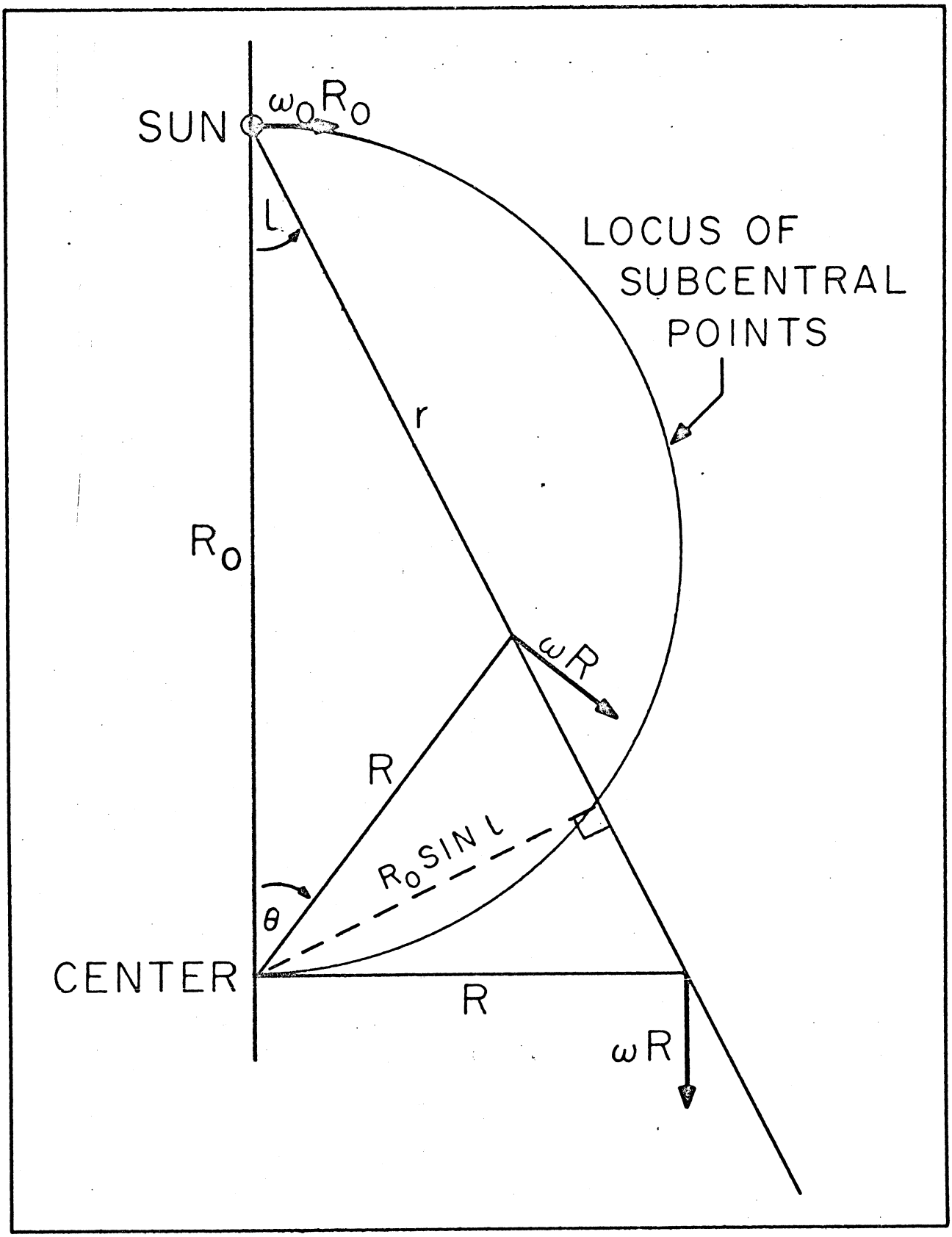
SUN
$\omega_0 R_0$
L
LOCUS OF
SUBCENTRAL
POINTS
r
R_0
ωR
R
$R_0 \sin L$
θ
CENTER
R
ωR

Figure 2.

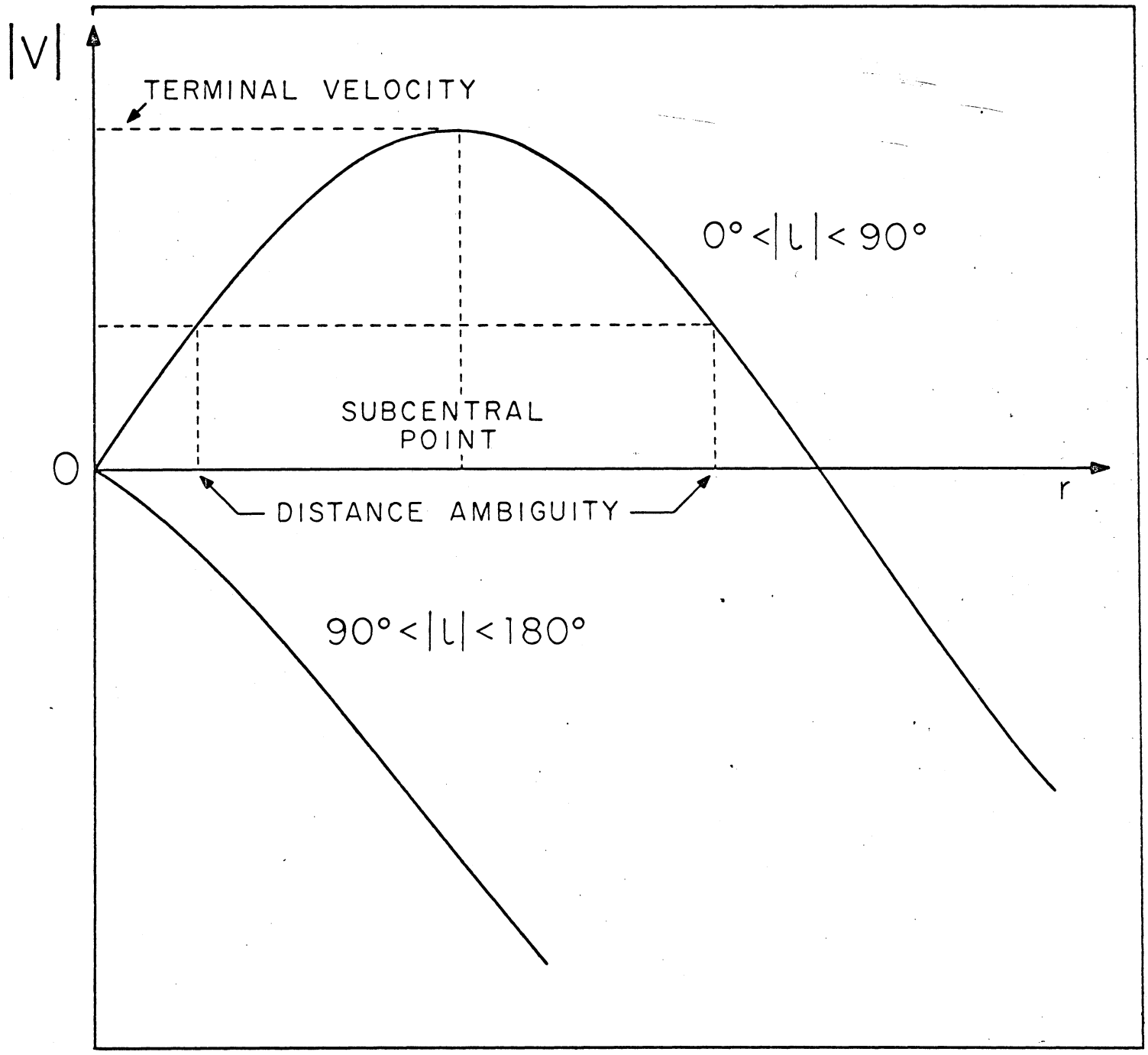
|V|
TERMINAL VELOCITY
0° < |l| < 90°
SUBCENTRAL
POINT
O
r
DISTANCE AMBIGUITY
90° < |l| < 180°

Figure 3.

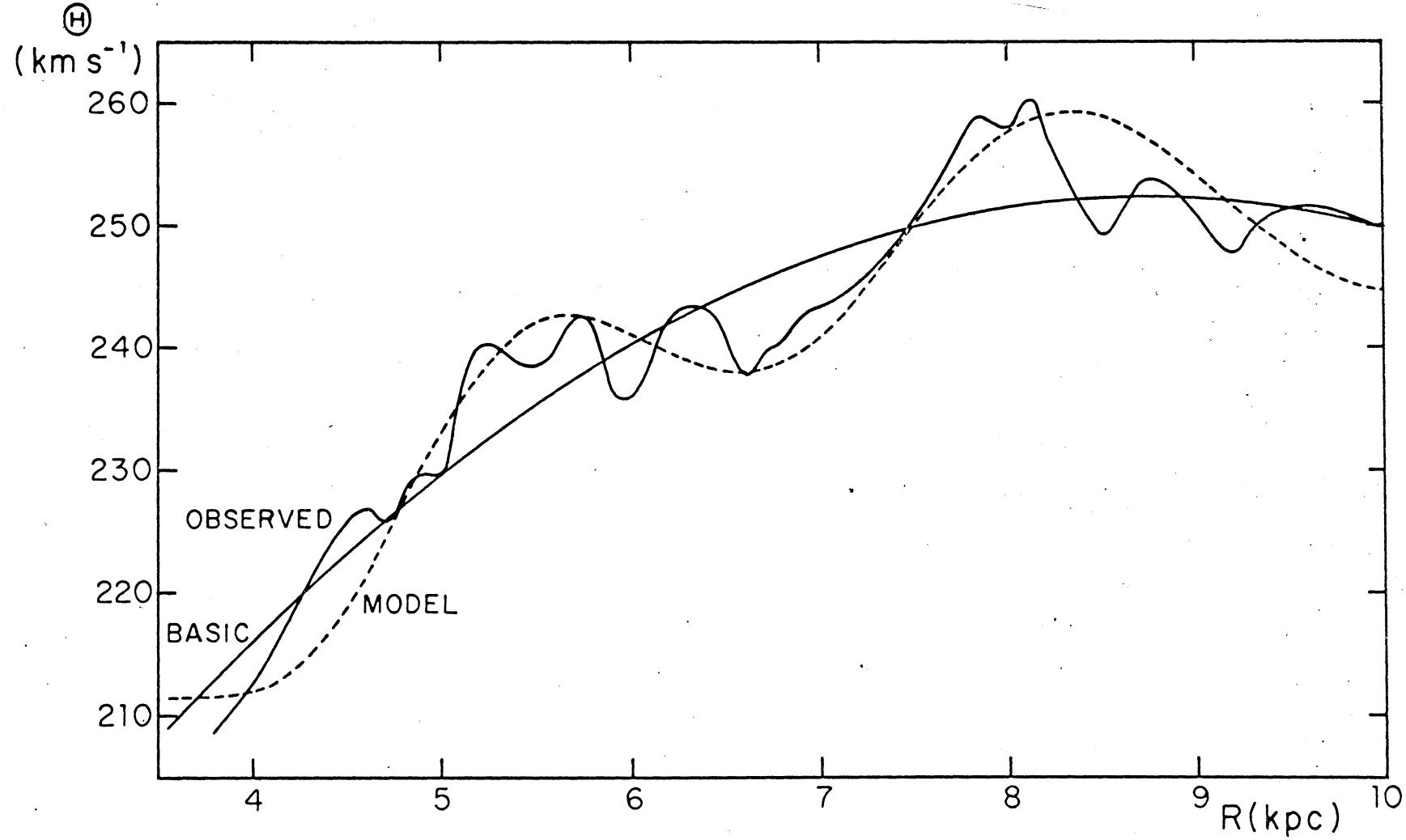
Θ (km s⁻¹)
260
250
240
230
220
210
OBSERVED
MODEL
BASIC
4
5
6
7
8
9
10
R(kpc)

Figure 4.

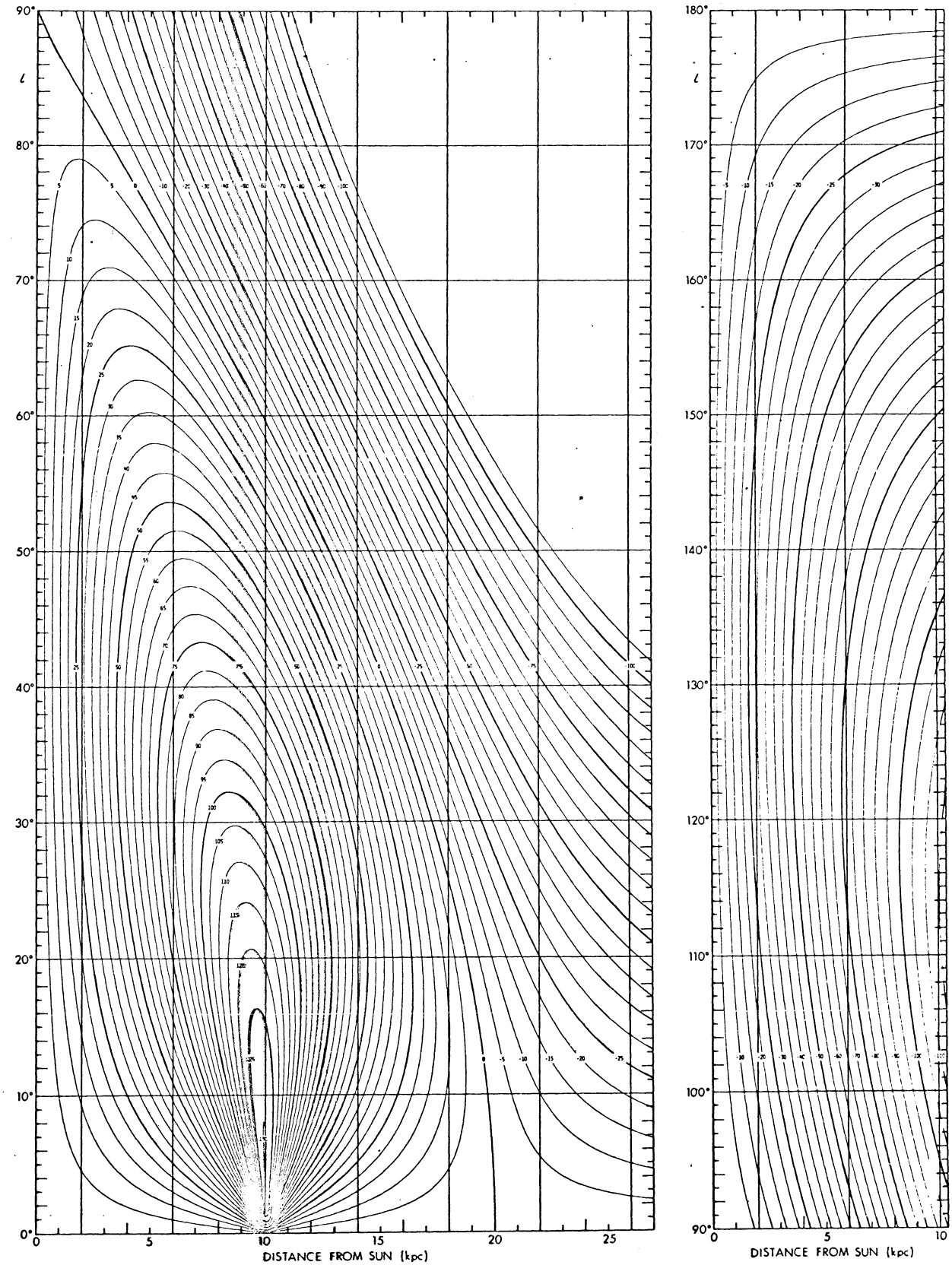
90°
80°
70°
60°
50°
40°
30°
20°
10°
0°
ℓ
0
5
10
15
20
25
DISTANCE FROM SUN (kpc)
180°
170°
160°
150°
140°
130°
120°
110°
100°
90°
ℓ
0
5
10
DISTANCE FROM SUN (kpc)

Figure 5.

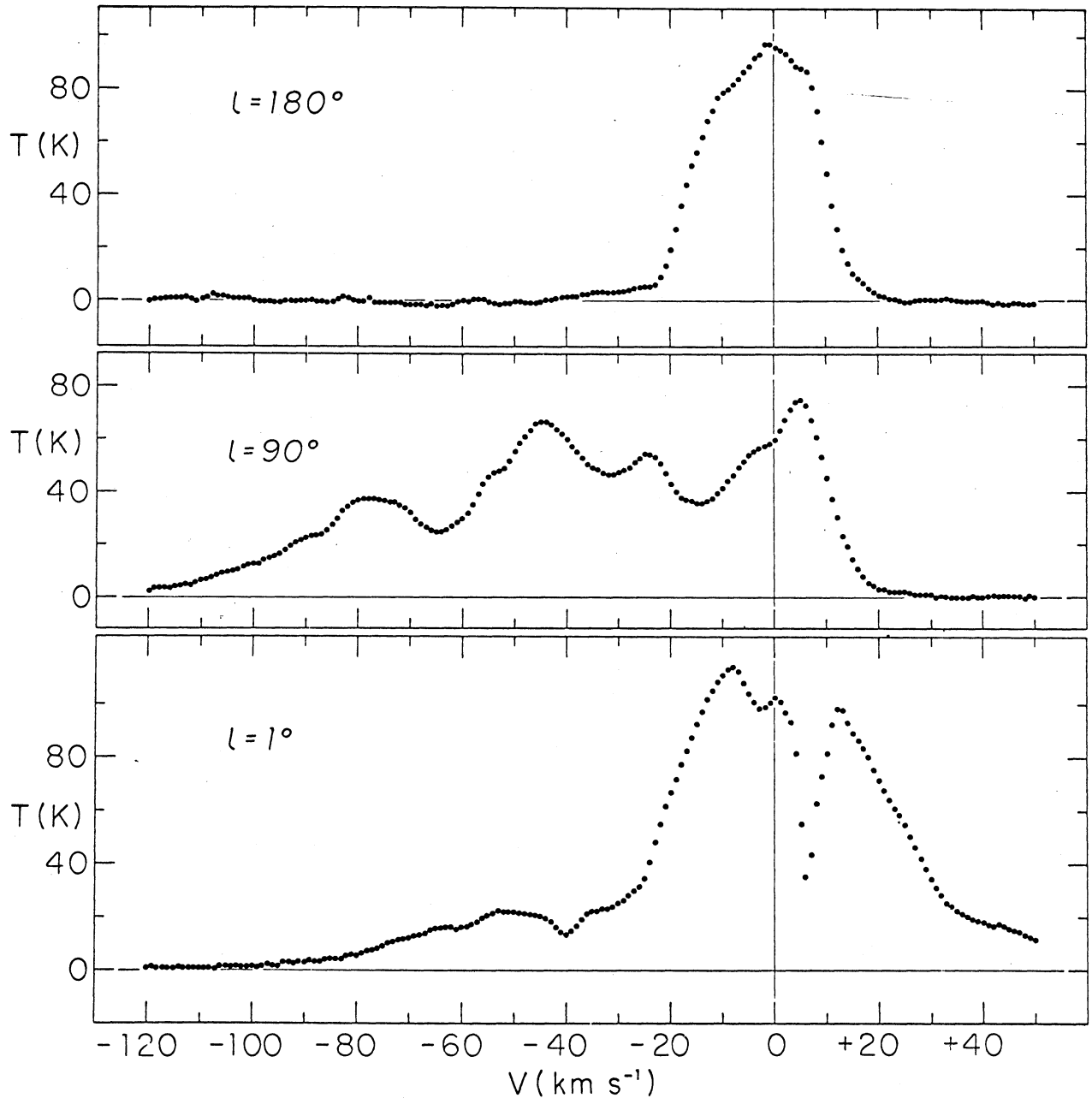

Figure 6.

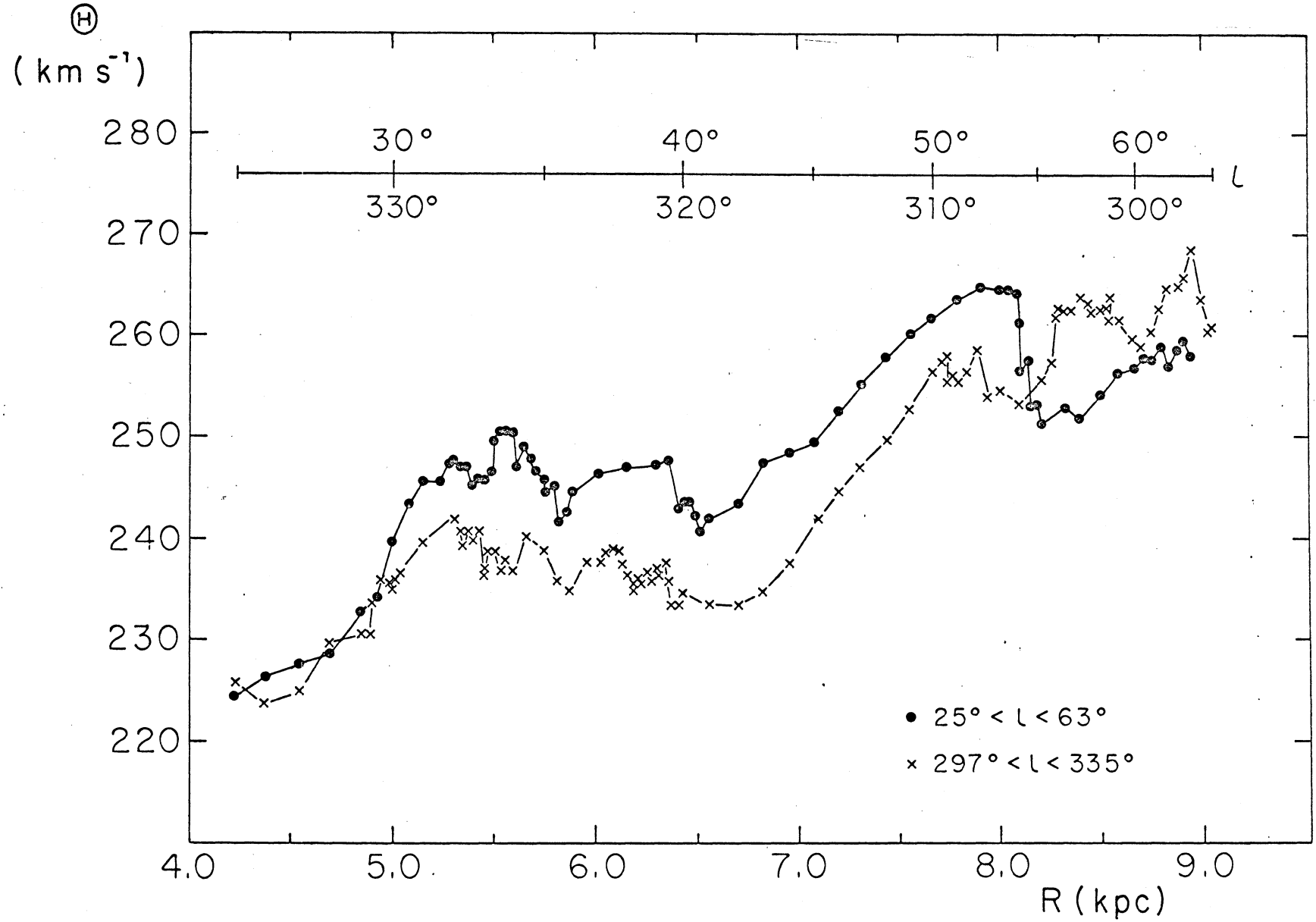
Θ
(km s⁻¹)
280
270
260
250
240
230
220
30°
40°
50°
60°
l
330°
320°
310°
300°
• 25° < l < 63°
× 297° < l < 335°
4.0
5.0
6.0
7.0
8.0
9.0
R (kpc)

Figure 7.

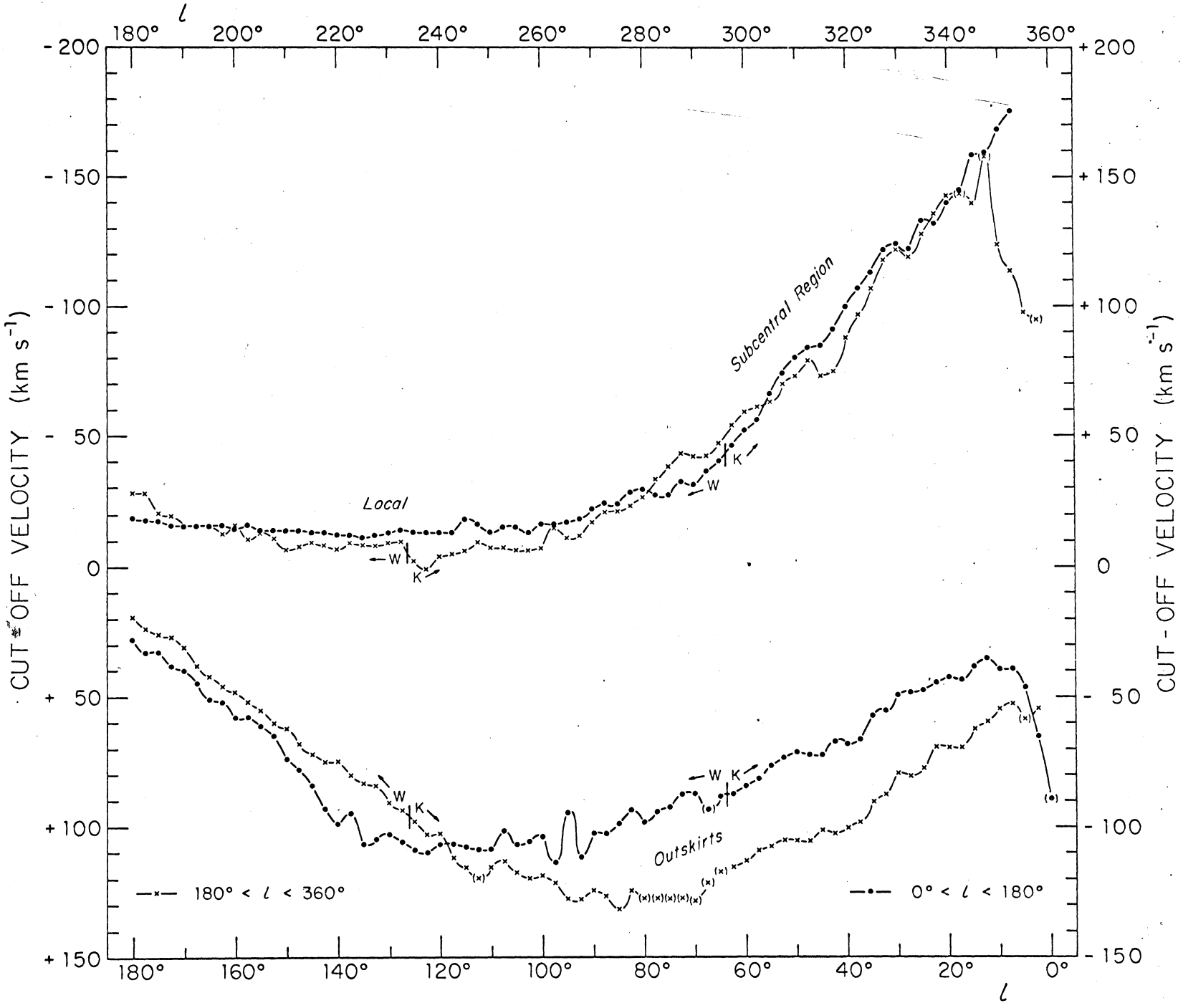
l
180°
200°
220°
240°
260°
280°
300°
320°
340°
360°
- 200
- 150
- 100
- 50
0
+ 50
+ 100
+ 150
+ 200
CUT-OFF VELOCITY (km s⁻¹)
Subcentral Region
Local
W
K
Outskirts
180° < l < 360°
0° < l < 180°
160°
140°
120°
100°
80°
60°
40°
20°
0°

Figure 8.

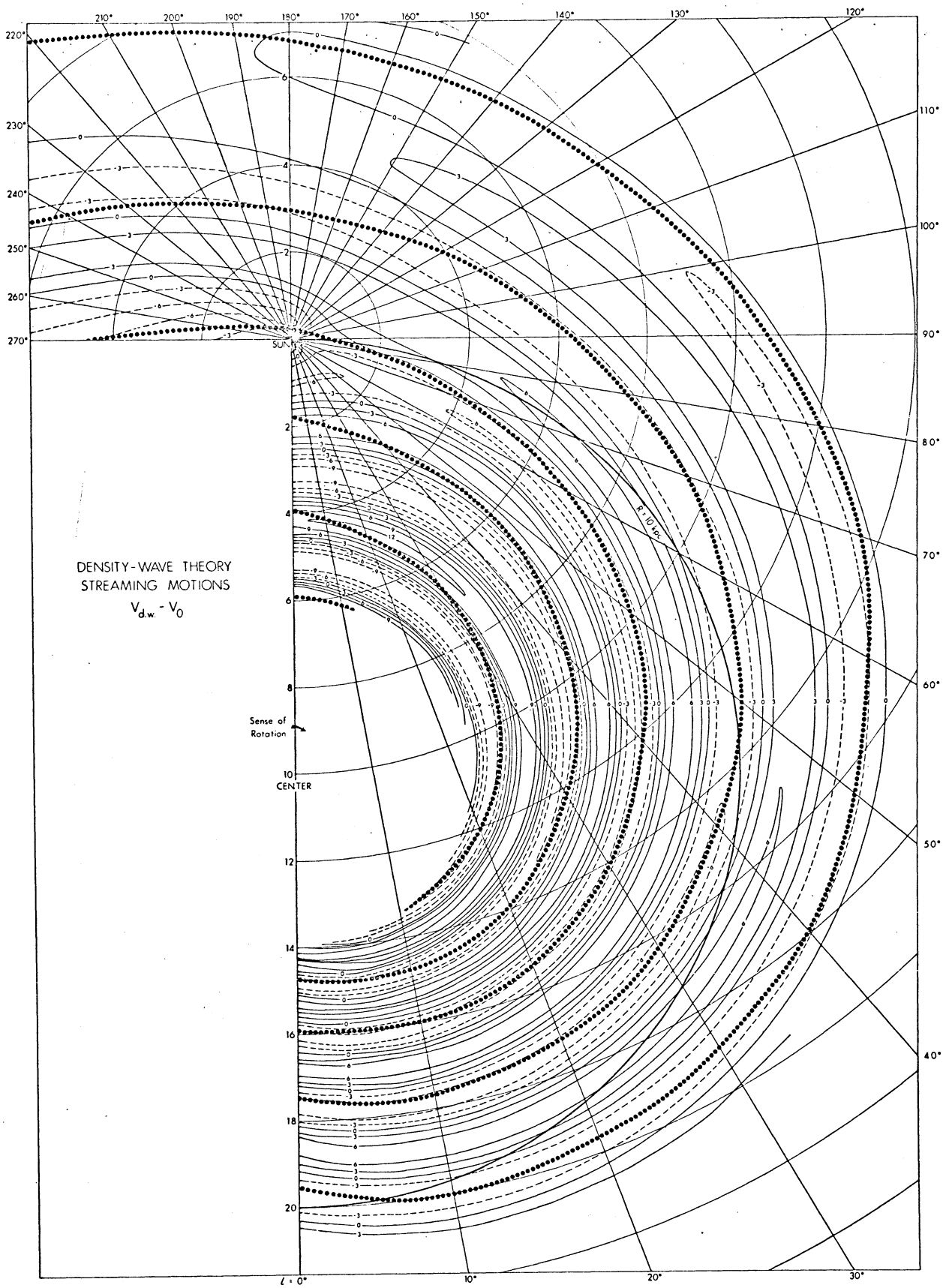
DENSITY-WAVE THEORY
STREAMING MOTIONS
$V_{d.w.} - V_0$
SUN
Sense of Rotation
CENTER
R = 10 kpc
$\ell = 0°$

Figure 9.

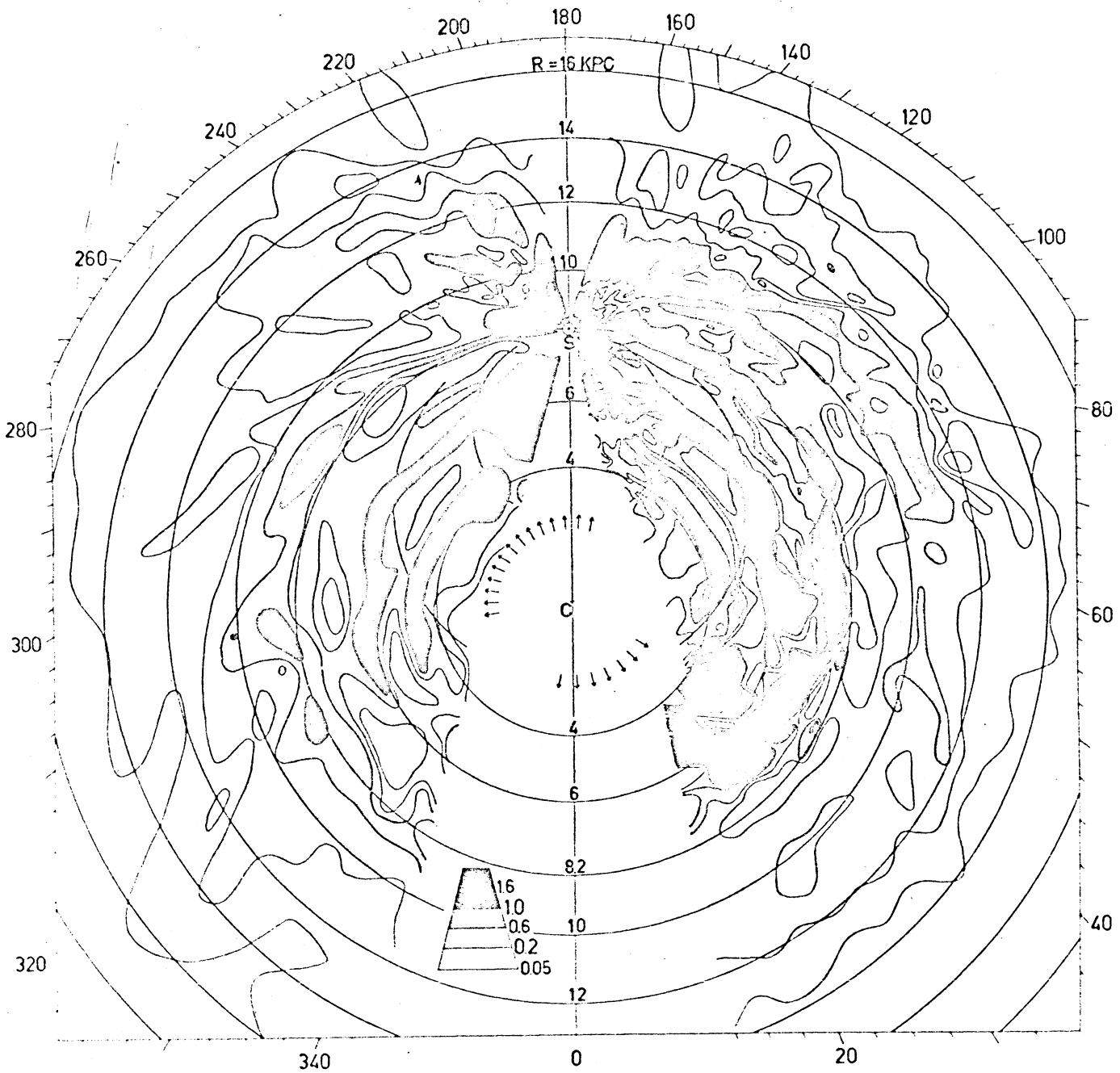
R = 16 KPC
180
200
160
220
140
240
120
260
100
280
80
300
60
320
40
340
0
20
14
12
10
S
6
4
C
4
6
8.2
10
12
1.6
1.0
0.6
0.2
0.05

Figure 10.

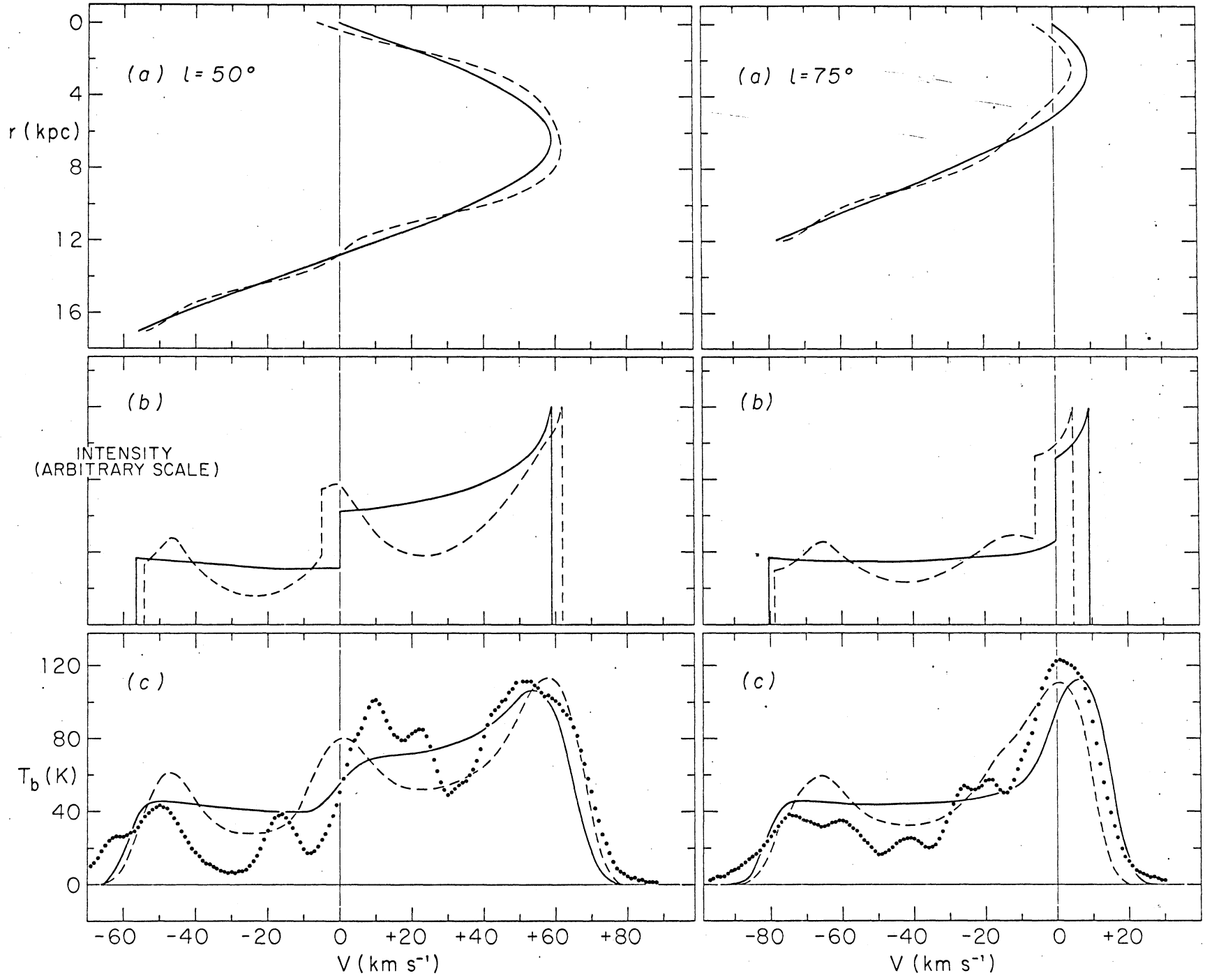
(a) l = 50°
(a) l = 75°
r (kpc)
0
4
8
12
16
(b)
INTENSITY
(ARBITRARY SCALE)
(c)
120
80
40
0
T_b (K)
-60 -40 -20 0 +20 +40 +60 +80
V (km s^{-1})
-80 -60 -40 -20 0 +20
V (km s^{-1})

Figure 11.

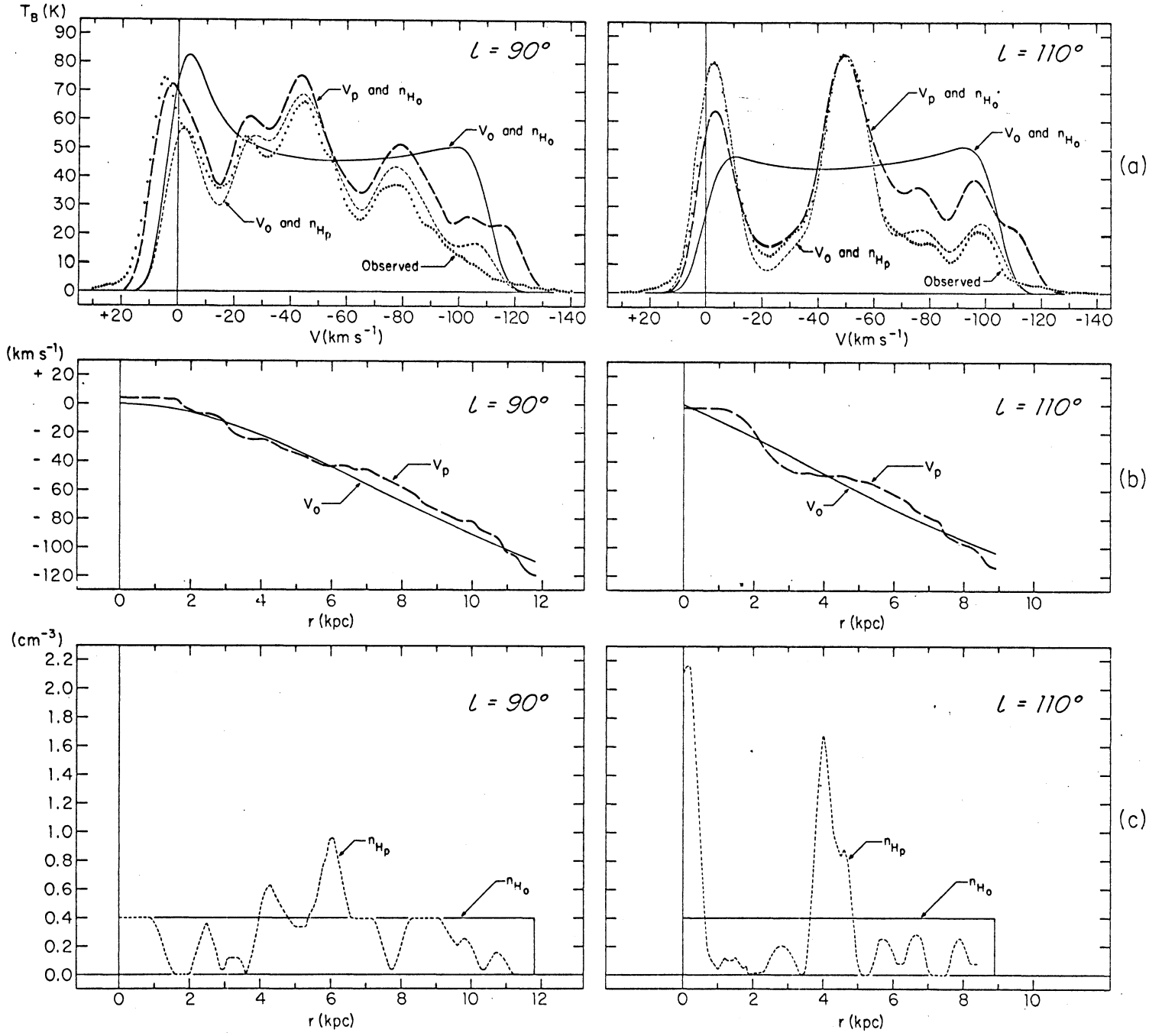
T_B (K)
l = 90°
l = 110°
V_p and n_{H_o}
V_o and n_{H_o}
V_o and n_{H_p}
Observed
V(km s^{-1})
(a)
(km s^{-1})
V_p
V_o
r (kpc)
(b)
(cm^{-3})
n_{H_p}
n_{H_o}
(c)

Figure 12.

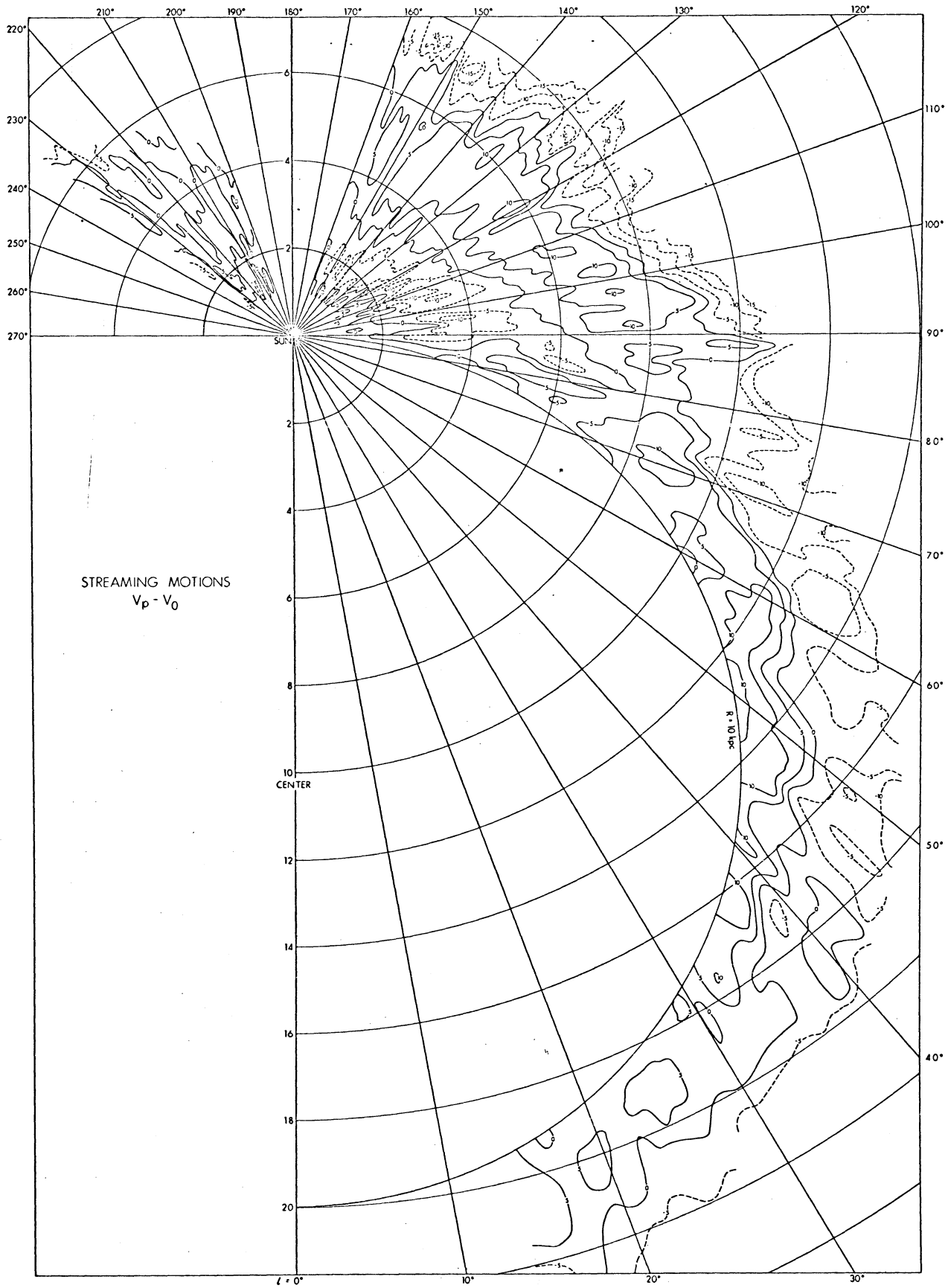
STREAMING MOTIONS
$V_p - V_0$
SUN
CENTER
R = 10 kpc
l = 0°
10°
20°
30°
210°
200°
190°
180°
170°
160°
150°
140°
130°
120°
110°
100°
90°
80°
70°
60°
50°
40°
220°
230°
240°
250°
260°
270°
2
4
6
8
10
12
14
16
18
20

Figure 13.

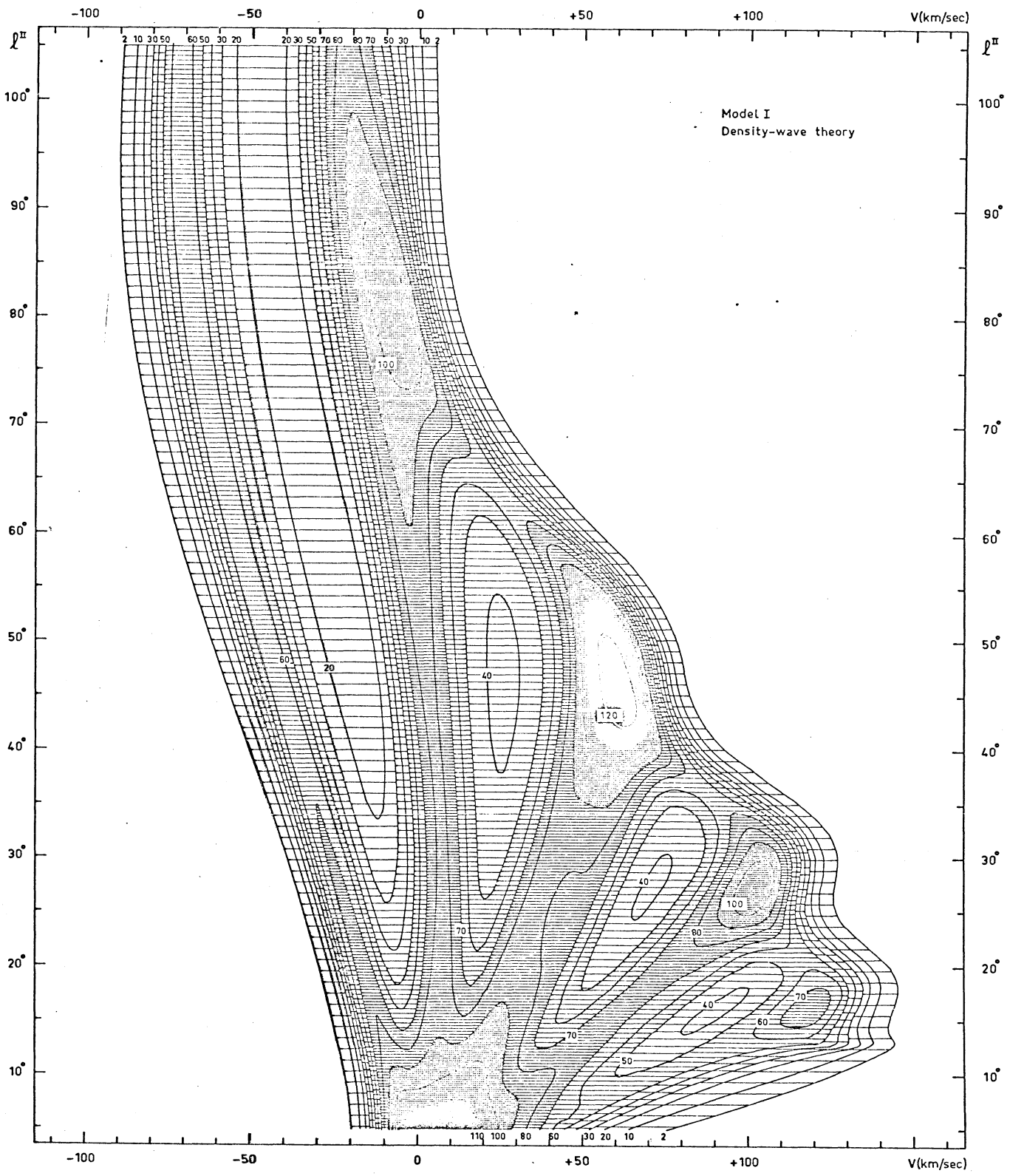
-100
-50
0
+50
+100
V(km/sec)
ℓ^{II}
100°
90°
80°
70°
60°
50°
40°
30°
20°
10°
Model I
Density-wave theory
2 10 30 50 60 50 30 20 20 30 50 70 80 80 70 50 30 10 2
100
60
20
40
120
40
100
80
70
40
70
60
70
50
110 100 80 50 30 20 10 2

Figure 14.

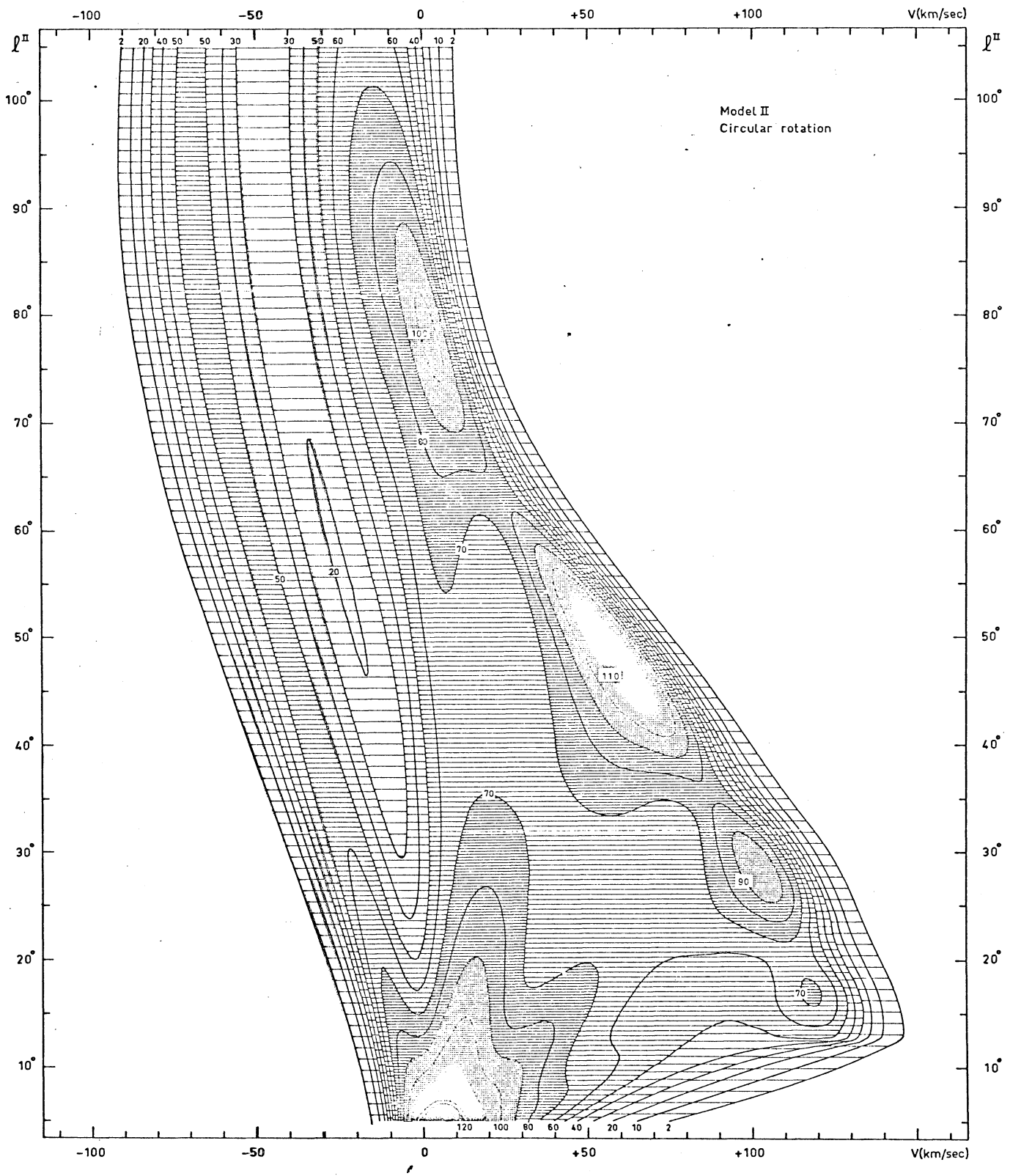
Model II
Circular rotation
V(km/sec)
l^{II}
-100
-50
0
+50
+100
100°
90°
80°
70°
60°
50°
40°
30°
20°
10°

Figure 15.

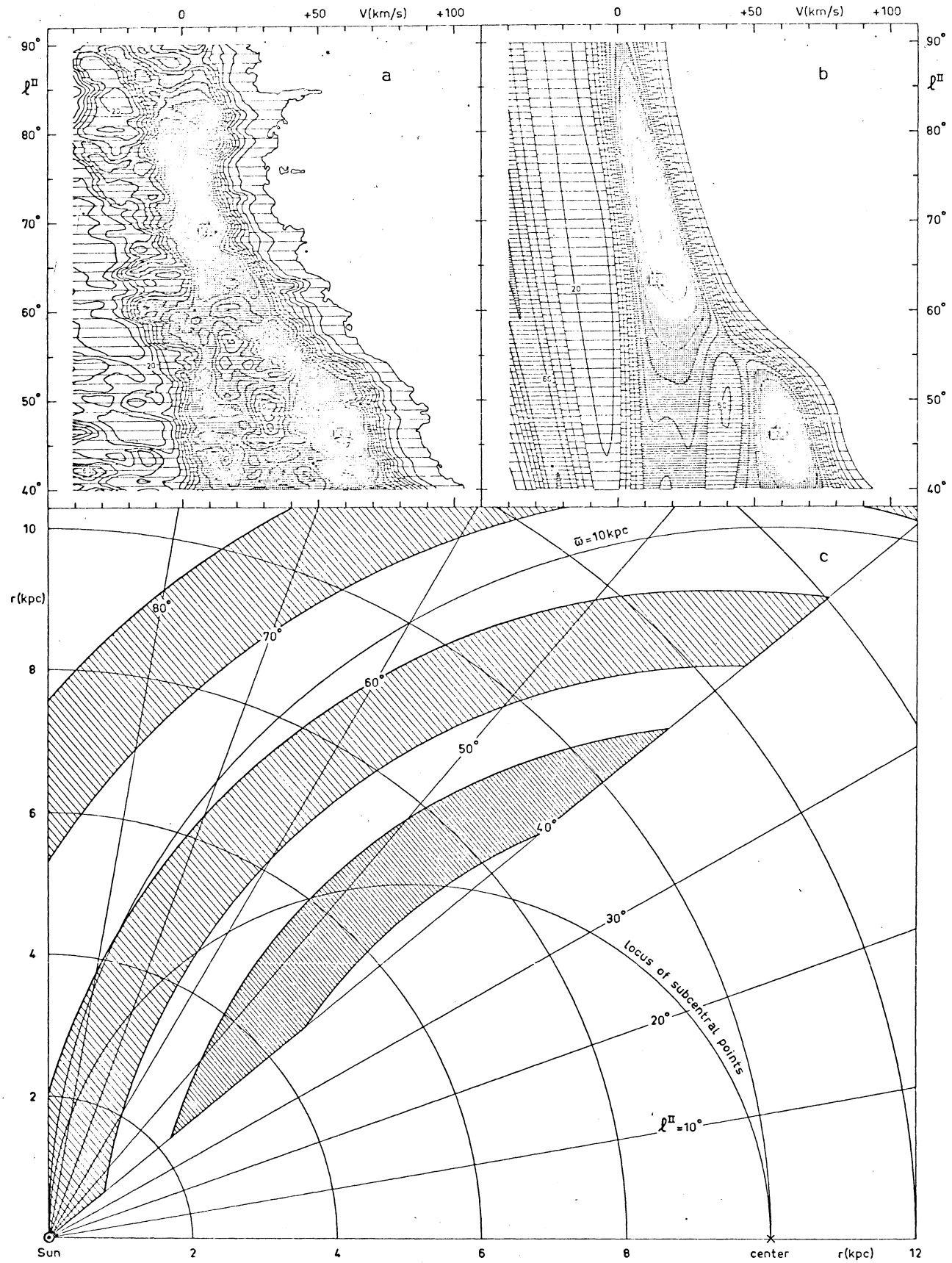
0
+50
V(km/s)
+100
a
b
ℓ^{II}
90°
80°
70°
60°
50°
40°
c
r(kpc)
10
8
6
4
2
$\bar{\omega}$=10kpc
80°
70°
60°
50°
40°
30°
20°
ℓ^{II}=10°
locus of subcentral points
Sun
2
4
6
8
center
r(kpc)
12

Figure 16.

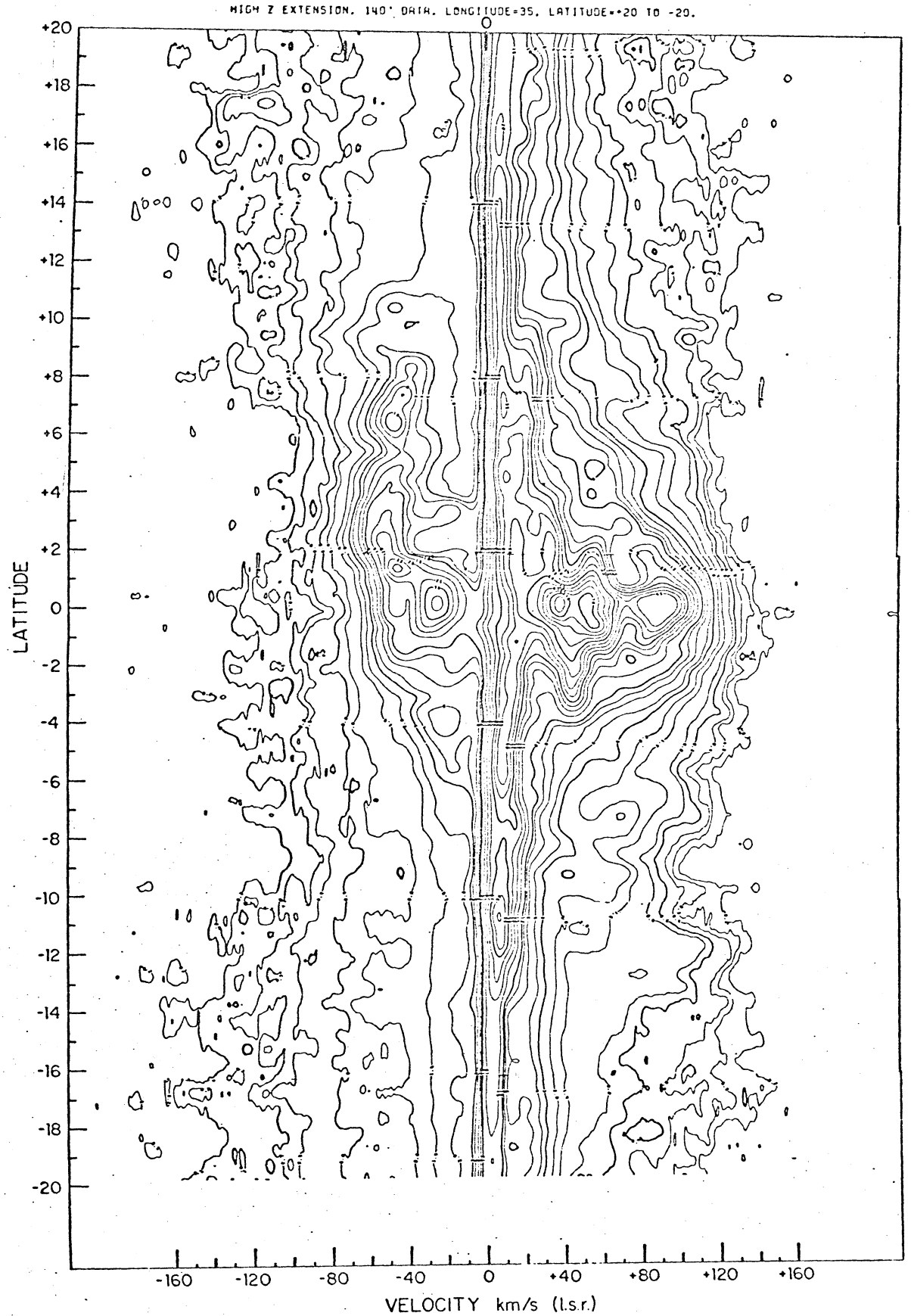

Figure 17. Preliminary figure!

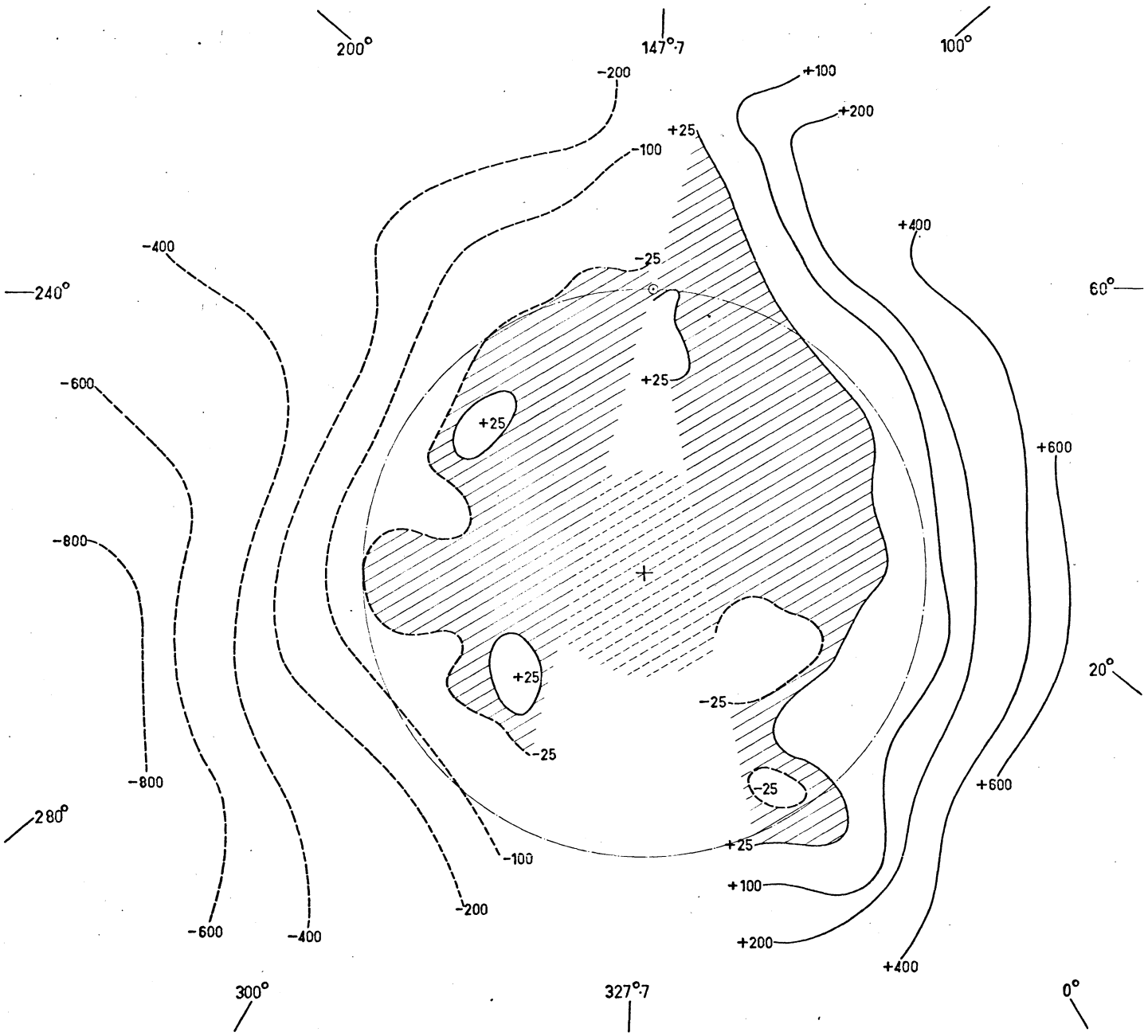
200°
147°.7
100°
-200
+100
+200
+25
-100
+400
-400
-25
240°
60°
+25
-600
+600
-800
+25
+25
-25
20°
-25
-800
+600
280°
-25
+25
-100
+100
-200
+200
-600
-400
+400
300°
327°.7
0°

Figure 18.

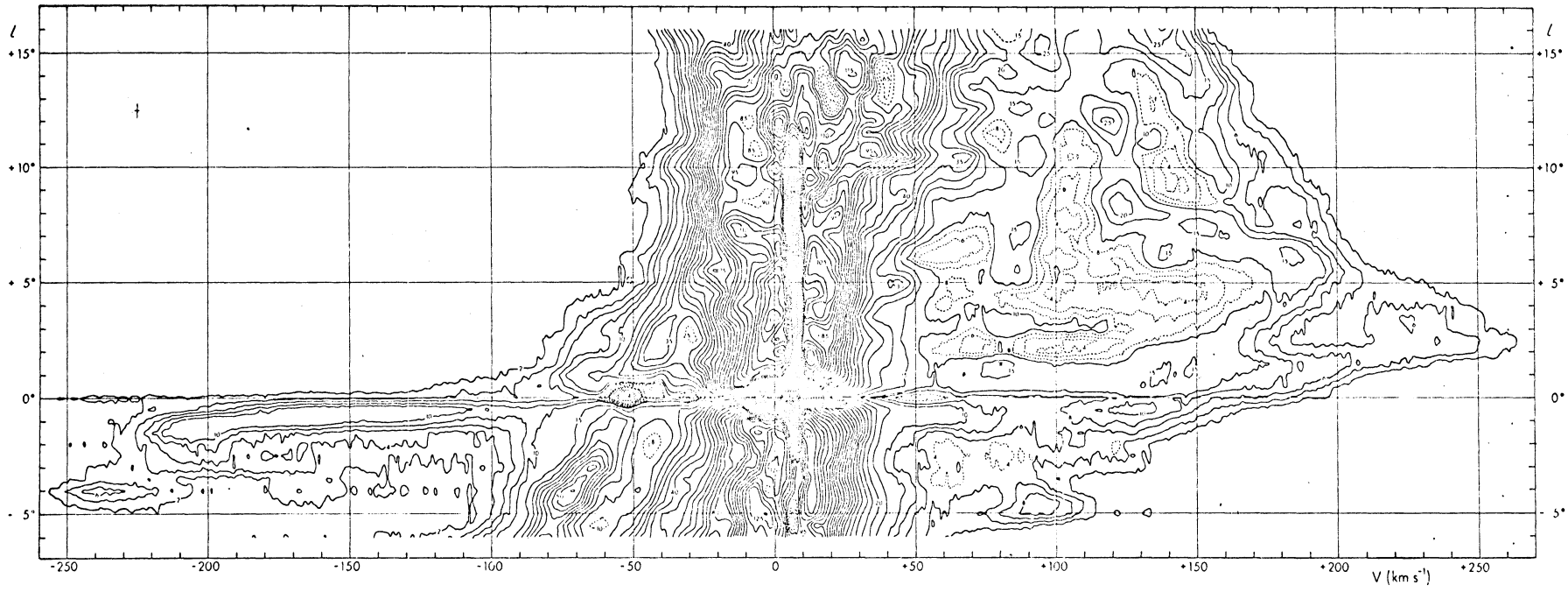

Figure 19.